PREPARED FOR THE U.S. DEPARTMENT OF ENERGY,
UNDER CONTRACT DE-AC02-76-CHO-3073

PPPL-2615
UC-420,424

PPPL-2615

LINEAR OPTIMAL CONTROL OF TOKAMAK FUSION DEVICES

BY

C.E. KESSEL, M.A. FIRESTONE, R.W. CONN

MAY 1989

PRINCETON
PLASMA PHYSICS
LABORATORY

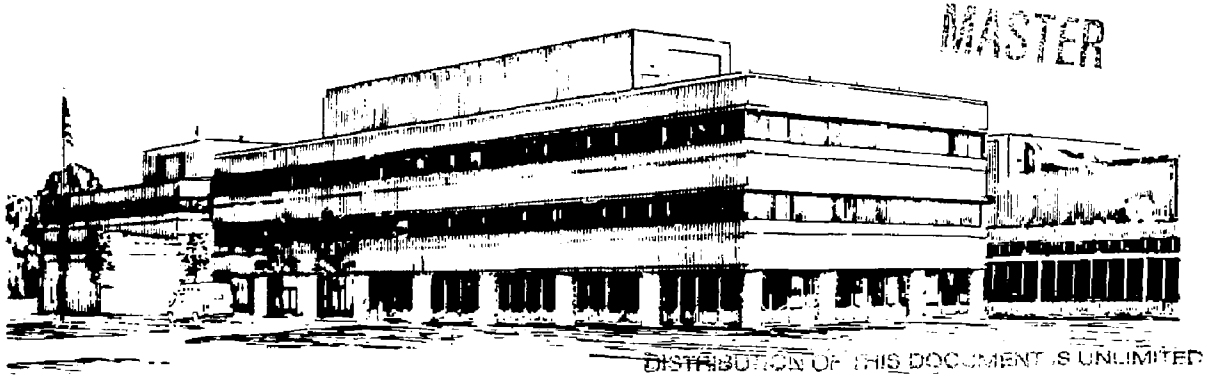

PRINCETON UNIVERSITY, PRINCETON, NEW JERSEY

NOTICE

Available from:

National Technical Information Service
U.S. Department of Commerce
5285 Port Royal Road
Springfield, Virginia 22161
703-487-4650

Use the following price codes when ordering:

Price: Printed Copy A04
Microfiche A01

DE89 011343

PPPL--2615

Linear Optimal Control of Tokamak Fusion Devices

C. E. Kessel[1], M. A. Firestone[2], R. W. Conn[3]

Princeton Plasma Physics Laboratory
Princeton University
P. O. Box 451
Princeton, New Jersey 08543

Abstract

The control of plasma position, shape and current in a tokamak fusion reactor is examined using linear optimal control. These advanced tokamaks are characterized by non up-down symmetric coils and structure, thick structure surrounding the plasma, eddy currents, shaped plasmas, superconducting coils, vertically unstable plasmas, and hybrid function coils providing ohmic heating, vertical field, radial field, and shaping field. Models of the electromagnetic environment in a tokamak are derived and used to construct control gains that are tested in nonlinear simulations with initial perturbations. The issues of applying linear optimal control to advanced tokamaks are addressed, including complex equilibrium control, choice of cost functional weights, the coil voltage limit, discrete control, and order reduction. Results indicate that the linear optimal control is a feasible technique for controlling advanced tokamaks where the more common classical control will be severely strained or will not work.

[1] Work was done while attending University of California, Los Angeles

[2] Mission Research Corporation, P.O. Drawer 719, Santa Barbara, California, 93102

[3] Institute of Plasma and Fusion Research and Mechanical, Aerospace, and Nuclear Engineering Department, University of California, Los Angeles, Boelter Hall, Room 6291, Los Angeles, California, 90024

1 Introduction

The control of tokamak plasma equilibrium is critical to achieving long duration plasma discharges. Virtually all control analyses in the tokamak literature have addressed the classical approach to the control of tokamaks because classical control is used in present experimental devices ([1]-[13]). However, the tokamak electromagnetic environment is highly coupled, and the modern optimal approach is better suited to deal with such a problem. The first serious modern optimal control analyses were done by Gran et al. ([14]-[15]) and Firestone[16], for radial position and plasma current control of the TFTR tokamak[13]. This device has a circular plasma and a thin structure (vacuum vessel) surrounding the plasma. Ogata and Ninomiya ([17]-[18]) also set up a modern control model for JT-60[19]. The present analysis is concerned with future tokamaks which will have important new features compared to present experimental devices, features which will impact how control is achieved.

In next generation and future tokamak reactors, the plasma will be surrounded by a thick blanket that is not likely to be up-down symmetric. The external ohmic and poloidal field coil locations will not be strictly determined by equilibrium considerations, but will also have to take into account engineering constraints such as coil maintenance, divertor or limiter ports, RF antenna structures, neutral beams, and diagnostics. These additional considerations may not allow up-down symmetric placement of coils and each coil would have to supply ohmic heating, vertical field, radial field, and shaping field. More complex equilibria may be necessary to achieve higher β_t and if divertors are used, control of the null point positions will be critical. Larger coil currents, voltages, and powers suggest that superconducting coils will be used. In addition, measurements will probably be scarce, with none or few taken inside the plasma chamber. The plasma density and temperature will be high, requiring that no contact be made with the first wall or other components not designed to handle the heat and particle loads.

The alterations beyond present experiments complicate the control problem and require a more accurate description of the system for control purposes. The classical control approach used on experimental machines is single-input/single-output ([5]-[7] and [13]). Control of a quantity is with one set (up-down symmetric pair) of coils. The coils are geometrically located to provide predominantly one function, either vertical field, radial field,

shaping field, or ohmic heating. Great effort is made in the design of the feedback system to avoid disturbing one parameter when controlling another. In addition, because of this control scheme, the coil-to-coil interactions (the voltage induced in one coil by another) are typically not included in the control model, and subsequently have to be minimized by the introduction of further circuitry[9]. Generally, some form of PID (proportional-integral-derivative) controller is used where the voltage, produced by the coil power supply, is proportional to a gain times the difference between the actual value of the parameter to be controlled and a reference value. This voltage is expressed as

$$V_{feedback} = k_p(y - y_r) + k_d(\dot{y} - \dot{y}_r) + k_i \int_0^t (y - y_r)dt. \qquad (1)$$

The terms k_p, k_d, and k_i are the gains for the proportional, derivative, and integral feedback control, respectively, and y represents the parameter to be controlled. The characteristics of advanced tokamaks are likely to strain this classical control philosophy.

Modern optimal control theory, specifically linear optimal control, can deal with the entire coupled electromagnetic environment including hybrid coil functions, electromagnetic interactions, sophisticated eddy current models, and complex equilibrium. The physical system is described by a set of ordinary differential equations, rather than the classical input-ouptut relations. Decoupling of the control system functions is not necessary because all the information has been included in the derivation of the gains, although it may still be useful for the given power supplies or control requirements. The feedback voltages are now represented as a gain matrix times a vector of the currents in the system (coil, plasma, and eddy currents). All the parameters are controlled simultaneously by all of the control voltages.

The tokamak control problem can be separated into two major parts, electromagnetic and plasma kinetic. The electromagnetic refers to controlling the magnetic and electric fields which maintain or change the plasma position, shape, and current. The plasma kinetic refers to controlling particle feed rates and heating to maintain or change the plasma density, temperature, current density, and their profiles. The two areas are ultimately coupled. Only the electromagnetic aspect will be examined, taking plasma kinetic parameters as known. The purpose of this work is to characterize the control of plasma position, shape, and current in advanced tokamaks and

to evaluate the feasibility of using linear optimal control. The INTOR[20] tokamak conceptual design is used as a reference example since it has many of the features envisioned for future tokamaks. It is not intended to design the control system for INTOR[20], but to use the design to examine control behavior. In Section 2, we outline the description of the tokamak electromagnetic environment. The operation of a tokamak and determination of the nominal trajectory are covered in Section 3. Linear optimal control of tokamaks is discussed in Section 4. The issues regarding application of linear optimal control are discussed in Section 5 and conclusions are presented in Section 6.

2 Tokamak Electromagnetic Environment

To utilize conventional optimal control theory, ordinary differential equations are required for the system description. This is accomplished using lumped parameter models. The LR circuit equations are used to describe the coupled behavior of the coils, plasma, and structure (eddy currents), represented by a vector differential equation,

$$\frac{d}{dt}\left[\underline{\underline{L}}\,\underline{I}\right] + \underline{\underline{R}}\,\underline{I} = \underline{V} \tag{2}$$

where $\underline{\underline{L}}$ is the matrix of self and mutual inductances, $\underline{\underline{R}}$ is the diagonal matrix of resistances, $\underline{I}$ is the vector of circuit currents, and $\underline{V}$ is the vector of circuit voltages. The plasma and eddy current circuits have no driving voltage since they are induced currents. The overall model of the electromagnetic environment is shown in fig. 1, using INTOR[20] as the example.

The plasma is modeled as a single filament located at the magnetic axis by using the semi-empirical formula,

$$R_m = R + \frac{a^2}{2R}\left(\beta_p + \frac{l_i}{2}\right) - \frac{a^3}{3R^2}\left(\beta_p + \frac{l_i}{2}\right)^2 \tag{3}$$

where R_m is the position of the magnetic axis, R is the plasma geometrical center, a is the horizontal minor radius, β_p is the poloidal beta, and l_i is the plasma internal self-inductance per unit length. The mutual inductances between the plasma and other circuits are determined using the filament

approximation for the plasma, although the plasma self-inductance and resistance are calculated including the full plasma dimensions.

$$L_p = \mu_o R \left(\ln \frac{8R}{a\sqrt{\kappa}} + \frac{l_i}{2} - 2 \right) \tag{4}$$

$$R_p = \frac{3.3x10^{-8} \alpha_n Z_{eff} R \ln \Lambda}{a^2 \kappa T^{\frac{3}{2}}} \tag{5}$$

T is the plasma temperature in keV, Z_{eff} is the effective charge number of the plasma including impurities, α_n is the trapped particle enhancement factor (taken as 2.0), $\ln \Lambda$ is the Coulomb logarithm, and κ is the plasma elongation.

The eddy currents actually compose a continuous current distribution in the tokamak structure. In order to use a lumped parameter description, the structure must be discretized to yield eddy current paths. Each one of these paths can then be treated as a single circuit. For the blanket zone surrounding the plasma, this is accomplished by breaking the blanket into three regions: the first wall; the breeder; and shield. These regions are characterized by their respective dimensions and electrical resistivities. The eddy currents are modeled as toroidally continuous strips. For the strip model, a thick structure is represented by a series of nested sheets or contours drawn through the center of the region to be modeled. These sheets are then segmented into strips, as illustrated in fig. 2. The dotted line around one of the strips shows the actual finite region that is being approximated. The strips are approximated as three filaments spaced across the length for mutual inductances and a solenoid for the self-inductance. The resistance is calculated using the full dimensions of the structure. The typical L/R time for a strip in the first wall is 7.5 ms., 1.0 second for the breeder, and 0.5 second for the shield.

Poloidal breaks which inhibit toroidally continuous currents are treated by increasing the resistance of the toroidally continuous eddy current strips. A full model including these breaks and their actual geometry explicitly would increase the system dimensions considerably[21], and is not considered necessary at this point. Thus the circuit model consists of 10 coil circuits, one plasma circuit, and 49 eddy current circuits, giving a total of 60 circuits.

The plasma circuit is allowed to move in response to magnetic fields present at its center, and is assumed to reach equilibrium instantaneously,

since the plasma balances itself in response to forces on the order of microseconds. The time derivative in the vector circuit equation can be expanded to give,

$$\underline{\underline{L}}\dot{\underline{I}} + \frac{\partial \underline{\underline{L}}}{\partial R}\underline{I}\dot{R} + \frac{\partial \underline{\underline{L}}}{\partial Z}\underline{I}\dot{Z} + \frac{\partial \underline{\underline{L}}}{\partial \kappa}\underline{I}\dot{\kappa} + \underline{\underline{R}}\underline{I} + \frac{\partial \underline{\underline{L}}}{\partial t}\underline{I} = \underline{V}. \tag{6}$$

Equilibrium of a dee-shaped plasma is represented by four nonlinear algebraic equations[22] describing the vertical field, radial field, quadrupole field, and hexapole field as functions of equilibrium parameters R, Z, κ, δ, I_p, β_p, and l_i, where δ, I_p, and Z are the triangularity, plasma current, and vertical distance from the midplane, respectively. These serve as the expressions giving R, Z, κ, and δ for given values of I_p, β_p, l_i, and external currents. These are given by,

$$B_Z = \sum_{i=1}^{N} f_i(R,Z;R_i,Z_i)I_i = \frac{\mu_o I_p}{4\pi R f(\kappa)}\left[\ln\frac{8R}{a} + \beta_p + \frac{l_i}{2} - \frac{3}{2} - \frac{a^2}{R^2}\left(\beta_p + \frac{l_i}{2} - \frac{1}{2}\right)\right] \tag{7}$$

$$B_R = \sum_{i=1}^{N} g_i(R,Z;R_i,Z_i)I_i = 0 \tag{8}$$

$$B_Q = a\sum_{i=1}^{N}\frac{\partial f_i}{\partial R}(R,Z;R_i,Z_i)I_i = \frac{\mu_o I_p}{4\pi R}\left[c_1\kappa^3 + c_2\kappa^2 + c_3\kappa + c_4 + c_5\beta_p\right] \tag{9}$$

$$B_H = \frac{a^2}{2}\sum_{i=1}^{N}\frac{\partial^2 f_i}{\partial R^2}(R,Z;R_i,Z_i)I_i = \frac{\mu_o I_p}{4\pi R}\left[c_6\frac{\delta}{\kappa^2} + c_7 + c_8\beta_p\right]. \tag{10}$$

The kernels f_i, g_i, $\frac{\partial f_i}{\partial R}$, and $\frac{\partial^2 f_i}{\partial R^2}$ represent the vertical, radial, quadrupole, and hexapole fields at the plasma center per unit current at the coil or eddy current. The constants c_1 through c_8, and the function $f(\kappa)$ are determined by fitting to several equilibrium calculations covering a range of values for the equilibrium parameters using the fixed/free boundary equilibrium code, NEQ[23]. This representation allows the gross plasma equilibrium parameters to be related directly to external currents, which is necessary for actual control of these parameters. The dependencies of the quadrupole and hexapole fields on l_i have not been resolved for this work, however they can be by using more equilibrium calculations. The plasma horizontal minor radius is taken to be constant, since a physically correct determination requires

a full equilibrium calculation. Two simple models are possible, toroidal flux conservation and a limiter contour constraint. The toroidal flux conservation is not satisfactory since it would indicate plasma size changes that are not consistent with the limiter or first wall location. The limiter constraint is not used because the processes describing the plasma contacting a limiter are not modeled. Thus it is considered most sensible to assume a constant horizontal minor radius, since it does not change much in the controlled simulations. The time derivatives $\dot{R}$, $\dot{Z}$, $\dot{\kappa}$, and $\dot{\delta}$ are then determined by differentiating the equilibrium equations, thereby assuming the plasma evolves through a series of equilibria. The plasma density, temperature, Z_{eff}, and l_i are specified functions of time.

3 Tokamak Operation

The INTOR[20] conceptual reactor design is used as the example for this study, although a new time dependent plasma start-up trajectory is derived. The limiter mode of operation is considered, but the horizontal minor radius is held constant. The predicted operation of an advanced tokamak can be broken into six regions; breakdown, start-up, ramp-up, flat-top, ramp-down, and RF current drive. The plasma current is chosen to follow the equation $I_p(t) = 12.0(1.0 - \exp^{-0.1155t})$ MA from 0.0 to 6.0 seconds, after which it is held constant at 6.0 MA. The breakdown and start-up regions of the discharge are taken to be from 0.0 to 0.3 seconds, the ramp-up region from 0.3 to 6.0 seconds, and flat-top for about 280 seconds. Only the ramp-up and flat-top regions are examined, as these comprise the region of tokamak fusion reactor operation over long periods of time. The ramp-down region is considered to be the reverse of the ramp-up.

The plasma trajectory is constructed as a finite number of equilibria. The equilibrium parameters are the plasma current, major radius, vertical position, horizontal minor radius, elongation, triangularity, poloidal beta, toroidal field, and plasma internal self-inductance. The evolution of some of these parameters as a function of time is shown in Table 1. An inverse MHD equilibrium calculation[23] determines the required coil currents at each of these points in the trajectory. In addition, the ohmic current necessary to drive the plasma current is calculated and distributed among the coils to minimize the vertical and radial fields in the plasma region. The resulting

field derivatives are also found to be small. The current in each coil at any time is the sum of the equilibrium and ohmic components. The coil current and voltage time trajectories are determined consistently with the following constraints: magnetic field at breakdown less than 5 gauss; coil voltages less than 50 kV; coil currents less than 50 kA/turn; coil current densities less than 20 MA/m^2; maximum $\dot{B}$ at the superconductor less than 5 T/sec; maximum B at the superconductor less than 8 Tesla; and 30 volts provided over the first 0.3 seconds for plasma breakdown and start-up. Each coil is assumed to have its own separate power supply, although power supply dynamics are not included. The trajectory does not include eddy currents, or additional voltages and currents incurred as a result of control.

4 Linear Optimal Control for Tokamaks

The nominal trajectory is the time-dependent path such that if the voltages $\underline{V}_o(t)$ are applied to the coils, the currents in the coils, plasma, and structure will follow the reference trajectories $\underline{I}_o(t)$, and the equilibrium parameters will follow their corresponding trajectories $R_o(t)$, $Z_o(t)$, $\kappa_o(t)$, and $\delta_o(t)$. However, the overall reference trajectory is based on an approximate model of the system, and any real application of these voltages would not in fact result in the nominal behavior. It is therefore necessary to construct a closed loop feedback controller which examines the present state of the system and provides a correction to the voltage to keep the plasma parameters at the nominal values. This requires a description of the perturbations to nominal values. The control is derived to keep these perturbations small, thereby keeping the system along its nominal path.

Five parameters are to be controlled: plasma current; major radius; vertical position; elongation; and triangularity. We define a vector of these five parameters as $\underline{Y}^T = [R, Z, \kappa, \delta, I_p]$. The currents in the system (coil, plasma, and eddy currents) are the state variables (the minimum number of variables that completely summarize the tokamak electromagnetic status), and the voltages on the coils are the control variables (the variables that are manipulated to generate the required state variables). The perturbations are described by linearizing the circuit, equilibrium, and velocity equations in a first order Taylor expansion:

$$\underline{I}(t) = \underline{I}_o(t) + \underline{I}_1(t) \tag{11}$$
$$\underline{V}(t) = \underline{V}_o(t) + \underline{V}_1(t) \tag{12}$$
$$R(t) = R_o(t) + R_1(t) \tag{13}$$
$$Z(t) = Z_o(t) + Z_1(t) \tag{14}$$
$$\kappa(t) = \kappa_o(t) + \kappa_1(t) \tag{15}$$
$$\delta(t) = \delta_o(t) + \delta_1(t). \tag{16}$$

The zeroth order terms describe the nominal trajectory, while the linear terms describe the perturbations to the currents, voltages, and controlled parameters. The resulting linear equations for the perturbed vector quantities are,

$$\dot{\underline{I}}_1(t) = \underline{\underline{A}}(t)\underline{I}_1(t) + \underline{\underline{B}}(t)\underline{V}_1(t) \tag{17}$$

and

$$\underline{Y}_1(t) = \begin{bmatrix} R_1(t) \\ Z_1(t) \\ \kappa_1(t) \\ \delta_1(t) \\ I_{p_1}(t) \end{bmatrix} = \underline{\underline{C}}(t)\underline{I}_1(t). \tag{18}$$

These linear equations provide a description of how the system behaves, and therefore indicate how deviations from the nominal can arise. In linear optimal control these equations are used to derive the closed loop feedback gains. The controller has all the information about the system and can more "intelligently" keep the system along nominal in spite of disturbances. The matrices $\underline{\underline{A}}$, $\underline{\underline{B}}$, and $\underline{\underline{C}}$ are described in Appendix A.

A function representing the system performance is needed to select the optimal control. The objective is to find the voltage corrections $\underline{V}_1$ which keep the perturbations of the controlled parameters $\underline{Y}_1$ near zero and which expend as little power as possible in doing so. The most common form for this so-called cost functional is the quadratic form,

$$J = \int_0^T \left[q_R(t)R_1^2(t) + q_Z(t)Z_1^2(t) + q_\kappa(t)\kappa_1^2(t) + q_\delta(t)\delta_1^2(t) + q_{I_p}(t)I_{p_1}^2(t) + \sum_{i=1}^{M} r_{ii}(t)V_{i_1}^2(t) \right] dt \tag{19}$$

or

$$J = \int_0^T \left[\underline{Y}_1^T(t)\underline{\underline{Q}}(t)\underline{Y}_1(t) + \underline{V}_1^T(t)\underline{\underline{R}}(t)\underline{V}_1(t)\right] dt \tag{20}$$

where the integral is over the time of control. The q terms are the weights for the controlled parameters and the r terms are the weights for the various coil voltages. The selection of these weights determines the time response of the controlled system. A quadratic form for the cost functional is not strictly necessary. However, it has intuitive appeal being similar to least squares, it often can be made proportional to the actual energy in the system, it verifies the truncation of the first order Taylor expansion by minimizing second order quantities, and, when coupled with linear dynamics, has a highly tractable solution (This is not true in most optimization problems[27]).

Succinctly, the optimization problem is to determine the control voltages that minimize the cost functional constrained by the linear dynamics described by Eq.(17), while leaving the controlled parameters, the circuit currents, and coil voltages unconstrained. This can be accomplished by constructing a Hamiltonian and using the calculus of variations ([24]-[27]) to derive the conditions for optimality. This is briefly covered in Appendix B. The minimization yields two primary results: the control $\underline{V}_1$ is given by a linear function of the currents $\underline{I}_1$; and is proportional through a matrix which is the solution to a differential matrix Riccati equation,

$$\underline{V}_1(t) = -\underline{\underline{R}}^{-1}(t)\underline{\underline{B}}^T(t)\underline{\underline{P}}(t)\underline{I}_1(t) \tag{21}$$

$$\underline{\underline{P}}(t)\underline{\underline{A}}(t) + \underline{\underline{A}}^T(t)\underline{\underline{P}}(t) - \underline{\underline{P}}(t)\underline{\underline{B}}(t)\underline{\underline{R}}^{-1}(t)\underline{\underline{B}}^T(t)\underline{\underline{P}}(t) + \underline{\underline{C}}^T(t)\underline{\underline{Q}}(t)\underline{\underline{C}}(t) = -\dot{\underline{\underline{P}}}(t). \tag{22}$$

It is important to note that the control voltages are not a function of the controlled parameters $\underline{Y}_1$, but of the currents $\underline{I}_1$. This result makes physical sense because the currents completely describe the electromagnetic environment, including the controlled parameters. This is one primary difference between optimal and classical control, and it has strong implications for the application of linear optimal control theory. This feedback control is illustrated in fig. 3.

In order to generate an optimal control the system matrices $\underline{\underline{A}}$, $\underline{\underline{B}}$, and $\underline{\underline{C}}$, and the weighting matrices $\underline{\underline{Q}}$ and $\underline{\underline{R}}$ are evaluated at a specific time along the discharge trajectory. They are then considered constant matrices (time-invariant). These matrices are used to derive the Riccati matrix $\underline{\underline{P}}$.

Since the control of the tokamak is to be performed for a period of time long compared to any system time scales, the upper limit in the cost functional integral is made infinite. This results in a steady-state Riccati matrix (time-invariant). The Riccati matrix is strictly valid only at the time the system and weighting matrices were evaluated. However, it is typical that the gain matrix $-\underline{\underline{R}}^{-1}\underline{\underline{B}}^{T}\underline{\underline{P}}$ will control well in an interval about the point in time that it was evaluated. This approach is referred to as a time-invariant, infinite-time output regulator [24]. For the simulations presented in the following, a constant gain matrix will be used to control the system for 200 ms. beyond the point in time where the matrices are derived. In order to control the entire discharge simulation a number of these gain matrices would be calculated at several points in time along the discharge trajectory, however this is not done in the present work. Short sections of the discharge are simulated to test the control.

The optimal control law requires that all the currents in the system be fed back. However, only the coil and plasma currents are measurable; the eddy currents are not. The remaining currents must be reconstructed from other measurements. In addition, the eddy current models are only discretized versions of the continuously distributed currents in the structure. More accurate models will require more eddy currents, and more currents would have to be reconstructed. This indicates it is unlikely to have as many measurements as currents (so that a unique relationship exists between them) because a very large number of measurements would be required. The consequence of this difficulty is that another form of estimation, such as the Kalman estimator ([24]-[27]), is needed to generate estimates of the currents from fewer measurements. This is of special interest for advanced tokamaks where the neutron and particle heating, as well as radiation damage, should make measurements near the plasma difficult. However, there are still too many currents to estimate and feed back for an on-line computer, even with the present model of 60 currents. There is thus motivation to derive a reduced system description that corresponds to fewer currents, and reduces the number of calculations required to determine the control.

5 Issues for the Optimal Control of Tokamaks

The control simulations are done by setting up initial perturbations in the coil, plasma, and eddy currents. The equilibrium corresponding to these currents is calculated to provide the controlled parameters, that have been perturbed from their nominal values. The system is then simulated using the derived optimal control gains. It is emphasized that the plasma density, temperature, l_i, and Z_{eff} are specified functions of time, and no effort has been made in this work to consider uncertainties in these parameters.

5.1 Weighting Matrices in the Cost Functional

The matrices $\underline{\underline{Q}}$ and $\underline{\underline{R}}$ in the cost functional are used to weight the various controlled parameters and voltages. There is no general method for choosing the matrices, although they have the most direct influence on the controlled behavior of the tokamak, and serve as design tools to achieve the desired responses. The matrices are virtually always diagonal, allowing the individual penalization of parameters and voltages. Increasing the values in $\underline{\underline{Q}}$ and/or decreasing the values in $\underline{\underline{R}}$ generally result in a faster return to nominal conditions. The greater the weight, the more heavily the corresponding variable is kept small. Thus if large values are chosen for the q terms in Eq.(19), then the system will only tolerate small values of $\underline{Y}_1$ and drive large values of $\underline{Y}_1$ quickly to zero. If the r terms are made large, then only small control action is used, taking longer for perturbations to be driven to zero.

Good control behavior can be qualitatively characterized by several features: smooth monotonic approach to nominal (no oscillations); short time to reach nominal; and modest, non-oscillating required voltage. The method used here to calculate the weights involves determining acceptable perturbations in the controlled parameters and available control[16]. For example, if it is acceptable for the plasma radial position to be 1 centimeter off the nominal value, then this represents the maximum tolerable perturbation. If only 10 kilovolts are available from the coil power supplies for the control, then this is the maximum available control. The weights are set equal to one over the square of these values, multiplied by factors to allow for fine tuning.

Thus, we have the expressions,

$$q_i = \frac{f_{Q_i}}{(\Delta Y_i)^2} \qquad r_i = \frac{1}{(f_{R_i} V_{o_i})^2} \tag{23}$$

for the values q_i and r_i which occur in Eq.(19). Once the ΔY_i's and V_{o_i}'s are set, the factors, f_{Q_i} and f_{R_i}, are varied to arrive at the desired response. The base values for the controlled parameters are as follows: 10^4 (ΔR=0.01 m); 10^6 (ΔZ=0.001 m); 10^4 ($\Delta\kappa$=0.01); 10^4 ($\Delta\delta$=0.01); and 10^{-8} (ΔI_p=10^4 amps). The base values for the control voltages are the reciprocal squares of the nominal voltages at that particular time in the discharge. When values are reported for the weights, they correspond to the f factors, not the actual weights.

Shown in fig. 4 are the major radius and vertical position for increasing values in the $\underline{\underline{Q}}$ matrix (which more heavily weight the controlled parameters). Three separate cases are shown, where the factors f_{Q_i} are all made 0.1, 1.0, and 10.0. One sees that the response is faster as the weights increase, although at the highest values oscillations (overshoot) are introduced. Decreasing the weights in the $\underline{\underline{R}}$ matrix would have a similar effect because the gains are being increased. These brief results illustrate the impact that the $\underline{\underline{Q}}$ and $\underline{\underline{R}}$ matrices have on the behavior of the controlled system, and should be kept in mind in the further discussions.

5.2 Voltage Limitation

An important concern in the control of disturbances is the limitation imposed by a maximum allowable voltage on the coils. This value has been taken as 50 kilovolts. In order to show the effects of such a limit, simulations were done at current flat-top, where the control voltages are the largest, with and without a voltage maximum imposed. It should be emphasized that all simulations presented do not have a voltage limit unless specified. We assume a perturbation in the plasma current of 0.5 MA, resulting in a 5 centimeter offset of the major radius. The response of plasma current and major radius are shown in fig. 5. The general effect is that the response is slowed. The major radius (as well as the elongation and triangularity which are not shown) does not overshoot in the voltage limited case, but more time is needed before the system returns to the nominal state.

This case constitutes a constrained voltage control problem. However, the optimal control has been derived assuming unconstrained voltages, thus the control is not truly optimal. A control solution taking the voltage constraints explicitly into account has not been done. Simulation results indicate that stability is maintained in all cases when a maximum voltage is imposed on the optimal control that was earlier derived assuming no voltage maximum. In fact, the responses are monotonic, and only take longer to reach the nominal state.

The voltage maximum plays an important role in the present work because control is being supplied purely by the large PF coils and these are far from the plasma. Smaller control coils close behind the shield would reduce the required voltages considerably. It is always desirable to locate the PF coils as close to the plasma as possible. Of course, if the coils are superconducting, it must be determined whether they can respond fast enough without exceeding their stability limits for magnetic field changes. For advanced tokamaks with a thick blanket, an inner coil set (right behind the shield) is likely to require mega-amps of current, while the outer PF coils carry 10's of mega-amps. Using normal coils for the inner set could result in severe power requirements. Finally, the location of the coils cannot be determined solely to produce a given class of equilibria, but is constrained by the engineering configuration of the device (ports, antennnas, diagnostics, etc.). Since the purpose of the present work is not to design the control system for INTOR[20], these issues are not pursued.

5.3 Effects of Eddy Currents

The presence of substantial structure between the poloidal field coils and the plasma introduces eddy currents which strongly affect the control. Present experimental devices have a very thin vacuum vessel with some coil and vessel support structure. The vessels are constructed with bellows (convoluted geometry) or insulator breaks to increase the resistance seen by toroidal currents. These reduce the eddy current amplitudes and L/R times. The vessels typically have a 5 ms. or smaller magnetic field penetration time. In other words, the structural components are configured with the purpose of minimizing eddy current effects. In the reactor, the blanket will be thick, with its structure and geometry dictated by neutronics, heat transfer/thermal hydraulics, and materials issues. The minimization of eddy current effects

will be a secondary concern.

To illustrate the effects of eddy currents and to demonstrate the difference between a thin structure, and a thick one, a series of start-up simulations have been done. Here the plasma current rises from zero to its final value in 300 ms. In fig. 6 the plasma current is shown as a function of time for the cases of no structure, toroidally continuous structure, and broken structure. The three broken structure cases are simulated by increasing the toroidally continuous eddy current resistances by a factor of 10, 100, and 1000. The toroidally continuous structure is unacceptable; the plasma current is a factor of 20 below the reference case after 300 ms. The coils are spending volt-seconds driving currents in the structure rather than the plasma, which would severely reduce the volt-seconds left for flat-top and ramp-down. From the broken structure examples an increase in the eddy current resistances by at least a factor of 100 is required to yield an acceptable response.

Breaking the blanket electrically to inhibit eddy currents is determined by the requirements of plasma start-up, and to a much lesser extent by plasma control. Due to the intense neutron and particle heating, as well as radiation damage, it is not desirable to electrically break the first wall and it is continuous in all simulations. Only the breeding region and shield are divided electrically, and the increase in the eddy current resistance by a factor of 100 is used in all subsequent simulations. The results indicate that the blanket must be electrically broken to drive plasma current ohmically in advanced tokamaks, unless the entire blanket is composed of high resistance materials (e.g., ceramic). Such a design also helps in control by reducing the eddy current disturbances.

Eddy currents also strongly influence control. This can be illustrated for a thick blanket by examining the response of the controlled parameters and coil voltages in two cases; no structure and full structure. The response of the major radius for full structure is shown in fig. 7, and is much slower than for no structure. Also in fig. 7 the voltage on one specific coil, #9, the outermost PF coil, is shown during this simulation. Initially the voltage is 7 times that with no structure, but later approaches as high as 1000 times the no structure result. On present machines, the no structure result would give a good approximation to the required voltage.

In addition to affecting control behavior, the eddy currents also present a physical limitation on the control of the parameters R, Z, κ, δ, and I_p, beyond those due to controller response time, measurement quality, and maximum

input (voltage). The eddy currents are induced in response to changes in coil and plasma currents, or plasma motion, and act to oppose the changes. The thicker and more conductive the structure, the more severe is the opposing action and the longer it persists. It is not possible to exercise control to any degree of accuracy and response time, because the eddy currents are tracking the current changes. This is well illustrated in figs. 8 and 9 where the vertical position and one eddy current amplitude are given as a function of time for a case where the weights on the controlled parameters are increased by a factor of 10 and 100. These increased weights would ideally correspond to cases of faster return to nominal. However, the vertical position shows larger oscillations for greater control authority. The eddy current amplitude oscillates because the control on the coils is oscillating in an effort to drive the system back to nominal more quickly. Clearly, this is not a desirable control, especially in a tokamak reactor where the plasma is hot. The plasma motion implied in figs. 8 and 9 would lead to contact with limiters and walls, possibly leading to a disruption. Smoother behavior is preferred and the control must be set to reflect the inherent limitations which eddy currents impose.

The examples in this section demonstrate the changing nature of the control problem as tokamak machines become more like fusion reactors. These changes require that we develop a more accurate system description for control which, of course, includes eddy currents. The philosophies now used for control in tokamak experiments will not suffice because they are based on a specific tokamak configuration that cannot be realized for fusion reactors.

5.4 Discrete Control

The actual implementation of optimal control in a tokamak will be in discrete, not continuous form. The tokamak plasma is continuous in time, but the control system is discrete because it requires that measurements be taken, signals processed, and control voltages generated. This requires a finite time. Thus control voltages are being updated every Δt, where Δt is the sum of all time delays. All simulations reported in this work so far assume continuous time control. To show that the control does not fail for finite time control updates, three discrete control cases are examined. This is done by using discrete analogues of the $\underline{\underline{A}}$ and $\underline{\underline{B}}$ matrices in the linear dynamics equation,

$$\underline{I}_1(t_{n+1}) = \underline{\underline{\dot{A}}}\underline{I}_1(t_n) + \underline{\underline{\dot{B}}}\underline{V}_1(t_n) \tag{24}$$

$$\underline{\underline{\dot{A}}} = \exp \underline{\underline{A}}\Delta t \tag{25}$$

$$\underline{\underline{\dot{B}}} = \left(\int_0^{\Delta t} \exp \underline{\underline{A}}\tau d\tau \right) \underline{\underline{B}}. \tag{26}$$

The time-invariant control problem is solved with sampling times of 1, 10 and 20 ms. The weighting matrices are taken to be those for the continuous-time case. The system is started at an initial perturbation, and the discrete control is such that the voltages on the coils are held fixed for the sampling time, Δt.

The responses of the plasma major radius and vertical position are shown in fig. 10 for each three discrete sampling times, 1, 10, and 20 ms. The 1 ms. case is almost identical to the continuous case, because this sampling time is shorter than all the system time constants. The 10 ms. case shows a similar response but a faster approach to nominal. For a sampling time of 20 ms., a much more oscillatory response is found. The vertical position shows violent oscillations, swinging from -8.0 to 8.0 centimeters before damping out. The major radius shows a fast initial approach to nominal, but overshoots.

The oscillatory behavior in the case of 20 ms. between sampling points is expected. The voltages to the coils are held constant for the sampling period, leaving the system to react without updating the control. The control must therefore push and pull more strongly when it is applied, in order to bring the system to nominal. Such behavior also implies that the coil voltages will make large swings back and forth, something which may not be feasible with a given power supply. This is supported by examining the voltage trajectories, shown in fig. 11. The 1 and 10 ms. cases show similar behavior while the 20 ms. case clearly shows an excessive effort to control the plasma.

A very interesting result appears in these simulations. The 10 ms. sampling time case shows faster approach to nominal than the 1 ms. case, and the return to nominal is monotonic. This illustrates that some discreteness in the application of the control may actually be desirable because of the presence of the eddy currents. The eddy currents introduce a time delay between the production of either an electric field for driving plasma current, or a magnetic field for maintaining equilibrium, and the arrival of these fields at the plasma. Since the eddy currents in the structure also slow down plasma

motion, shape, and current changes, it should not be necessary to update the control more frequently than the time delay. Thus a system response can be obtained that is as good as that of the continuously controlled system by using a sampling time that is of the order of the eddy current delay time.

The controllers on present tokamak experiments have sampling times between 2 to 10 ms. and the eddy current time scales for the vacuum vessel are typically 5 ms. The results here suggest that future tokamaks with thick blankets may be better and more efficiently controlled using a discrete controller and a sampling period on the order of the eddy current time scale. The final choice of sampling period will depend on the power supply dynamics and the on-line computer requirements, neither of which have been modeled in these simulations.

5.5 Reduction of System Order

Reduction of the system order is desirable for practical implementation of a controller and estimator. The optimal control law specifies the control as a linear function of the circuit currents. Yet while the coil and plasma currents can be measured, the eddy currents cannot. The eddy currents must in turn be estimated from available measurements, perhaps using the Kalman estimator ([24]-[27]). In addition, the larger the number of circuits in the system model, the longer will be the required computational time for both the controller and the estimator. Therefore, order reduction is desirable and must be done in a manner that has little or no influence on the true system response.

A modal reduction method is developed in which those modes with unstable and near-zero eigenvalues, as well as dominant negative eigenvalues, are retained in the reduced-order model. This technique can guarantee stability of the linear closed loop system. The reduced-order model has modal states as variables which do not correspond directly to currents in the original system. The modal state currents are used to derive the optimal control (or system gains). The control derived in this way is then applied to the larger, original system. A number of other order reduction techniques were considered, but were not found to guarantee stability of the closed loop system, or were not applicable to unstable open loop systems[28]. A description of the modal reduction technique is given in Appendix C.

There are a number of characteristics of advanced tokamaks that mo-

tivate order reduction. Tokamaks of advanced design are unstable due to the vertical instability caused by plasma elongation. The system usually has near-zero eigenvalues because of the use of superconducting coils, which have zero resistance. Furthermore, such tokamaks have many large negative eigenvalues corresponding to the eddy currents. For instance, in the case of *INTOR*[20] studied here, the full-order closed loop linear system matrix has at least 40 of its eigenvalues unchanged from the open loop values (these are the largest negative eigenvalues), and the eigenspectrum shows a natural break at the 12^{th} eigenvalue (when arranged from largest to smallest) where the eigenvalues jump by a factor of between 20 and 300.

The unstable and near-zero eigenvalues must be included in the reduced-order model to insure that the control is stabilizing. The fact that 40 eigenvalues are unchanged from open loop to closed loop systems suggests that these modes are not affected by the control since they already decay fast enough. These eigenvalues can be neglected in a reduced-order model. Another key is that the break in the eigenspectrum, which represents the difference between the coil and plasma, and eddy current time scales, suggests where a reduction ought to take place. These points all indicate that a reduction can indeed be made and will yeild controlled behavior very similar to full-order control of the system.

Two examples are shown in figs. 12 and 13 which illustrate order reduction. The original system is modelled with 60 states while the reduced-order models have 13, 15, and 20 states, respectively. The weights are chosen to be the same in the three cases, and the same initial perturbations are used in all cases. A 12 state case could not be simulated because the oscillatory behavior is too violent. The responses for the 13 state case are poor. This is primarily due to the absense of control over the fine time scale behavior. For the 15 state case the response behavior is much improved, although there are discrepancies due to long time scale oscillations. Finally, the 20 state case gives results almost identical to the full-order results.

These examples indicate that it is feasible to use a reduced order model which requires fewer states to be estimated and fed back, to model and control the full-order system. If a more accurate eddy current model is used (for example, to include poloidal breaks explicitly), then it only introduces more of the larger negative eigenvalues which correspond to the currents neglected in the reduced order model. Thus the reduced-order model should still be valid.

6 Conclusions

Linear optimal control of advanced tokamaks is examined and demonstrated to be a feasible candidate for controlling the electromagnetic environment. It is particularly well suited for advanced tokamaks, such as INTOR[20] or reactors, where eddy currents have a much greater effect on the system. The additional features of advanced tokamaks are likely to strain the classical single-input/single-output strategy. The linear optimal control approach is based on a total system description which includes accurate models of the dynamics. In fact, it is not the optimal part of the control that is critical but the ability of the control to deal with the entire coupled system. This includes multiple-input/multiple-output and control of all parameters simultaneously, rather than the scalar decoupled control of the classical approach. The optimization serves as the best way to choose the gains, and guarantees a stable linear closed loop system.

Optimal control will allow the actual control of equilibrium parameters, rather than requiring a preprogramming of the coil currents assuming expected plasma parameters. The multipole method employed in this paper gives a relationship between equilibrium parameters and the currents in the plasma and the external conductors. The control voltages are a function of the currents, which determine the equilibrium configuration. It is not necessary to measure equilibrium parameters such as elongation and triangularity, which are required for classical control. The optimal control approach also can handle more complicated equilibria, such as beans, asymmetric plasmas, and divertor plasmas. Rather than controlling the equilibrium parameters, the magnetic flux or field at several probes could be controlled simultaneously.

The important limitations in the control of advanced tokamaks, aside from those of the coil power supply response time and measurement quality, are the coil voltage limit and eddy currents. These limitations reduce the speed and smoothness with which a perturbation can be returned to nominal. Voltage limits lead to slower returns to nominal, although they do eliminate any overshoot. It should be pointed out that the voltage limit can be dealt with by making the weights on the coil voltages in the cost functional large enough to avoid exceeding the limits. This would remove the concern over stability, but would influence control behavior.

It is clear that the complexities caused by the presence of structure (eddy

currents) in advanced tokamaks will be more severe than in present experiments. It has been shown in this work that while the first wall can be electrically continuous, the blanket must be divided in order to increase the eddy current resistances by at least a factor of 100. This will aid control, although the control will still return perturbations to nominal more slowly than for a thin structure. Attempts to achieve very fast response of the control leads to highly oscillatory responses as the controller tries to compensate for exclusion of the fields by the eddy currents.

Discrete control would actually be used in real devices, with the sampling time determined by the time delays in activating coil power supplies. It appears from the simulations reported here that there are advantages to controlling discretely using a sampling time on the order of the eddy current decay time, rather than using very short sampling times. Fast monotonic approaches to nominal are found and the required coil voltages are not much different from those predicted from the continuous time cases.

Finally, the issue of reducing the order of the system model has been addressed. Reduction of system order is critical to real implementation of linear optimal control in tokamaks, because the models will in general require many circuits to describe the eddy currents in the structure. A modal reduction technique has been found to be the only approach which guarantees stability of the closed loop system. For a system such as INTOR[20], 20 modal states are required to reproduce the behavior of the full-order (60 state) system. The model of the tokamak electromagnetic environment yields many large negative eigenvalues which correspond to the eddy currents. The introduction of more eddy currents to produce a more accurate model only introduces more modes with large negative eigenvalues, which can be neglected. This indicates that even if the system order is increased, the reduced system will still be accurate. System reduction means in practice a significant reduction in the computer time required for estimation and voltage calculations.

Appendix

A Linearization

The application of linear optimal control requires a linearized model of the actual nonlinear mathematical description of the physical system. The time dependence of terms will be suppressed in the following. The nonlinear dynamics model is given by the vector circuit equation, equilibrium equations, and velocity equations.

$$\underline{\underline{L}}\dot{\underline{I}} + \frac{\partial \underline{\underline{L}}}{\partial R}\underline{I}\dot{R} + \frac{\partial \underline{\underline{L}}}{\partial Z}\underline{I}\dot{Z} + \frac{\partial \underline{\underline{L}}}{\partial \kappa}\underline{I}\dot{\kappa} + \underline{\underline{R}}\underline{I} + \frac{\partial \underline{\underline{L}}}{\partial t}\underline{I} = \underline{V} \tag{27}$$

$$\underline{w}_R^T\underline{I} = 0 \tag{28}$$

$$\underline{w}_Z^T\underline{I} = 0 \tag{29}$$

$$\underline{w}_\kappa^T\underline{I} = 0 \tag{30}$$

$$\underline{w}_\delta^T\underline{I} = 0 \tag{31}$$

$$\frac{\partial \underline{w}_R^T}{\partial R}\underline{I}\dot{R} + \frac{\partial \underline{w}_R^T}{\partial Z}\underline{I}\dot{Z} + \frac{\partial \underline{w}_R^T}{\partial \kappa}\underline{I}\dot{\kappa} + \dot{\underline{I}}^T\frac{\partial \underline{w}_R}{\partial \underline{I}}\underline{I} + \underline{w}_R^T\dot{\underline{I}} + \frac{\partial \underline{w}_R^T}{\partial t}\underline{I} = 0 \tag{32}$$

$$\frac{\partial \underline{w}_Z^T}{\partial R}\underline{I}\dot{R} + \frac{\partial \underline{w}_Z^T}{\partial Z}\underline{I}\dot{Z} + \underline{w}_Z^T\dot{\underline{I}} = 0 \tag{33}$$

$$\frac{\partial \underline{w}_\kappa^T}{\partial R}\underline{I}\dot{R} + \frac{\partial \underline{w}_\kappa^T}{\partial Z}\underline{I}\dot{Z} + \frac{\partial \underline{w}_\kappa^T}{\partial \kappa}\underline{I}\dot{\kappa} + \dot{\underline{I}}^T\frac{\partial \underline{w}_\kappa}{\partial \underline{I}}\underline{I} + \underline{w}_\kappa^T\dot{\underline{I}} + \frac{\partial \underline{w}_\kappa^T}{\partial t}\underline{I} = 0 \tag{34}$$

$$\frac{\partial \underline{w}_\delta^T}{\partial R}\underline{I}\dot{R} + \frac{\partial \underline{w}_\delta^T}{\partial Z}\underline{I}\dot{Z} + \frac{\partial \underline{w}_\delta^T}{\partial \kappa}\underline{I}\dot{\kappa} + \frac{\partial \underline{w}_\delta^T}{\partial \delta}\underline{I}\dot{\delta} + \dot{\underline{I}}^T\frac{\partial \underline{w}_\delta}{\partial \underline{I}}\underline{I} + \underline{w}_\delta^T\dot{\underline{I}} + \frac{\partial \underline{w}_\delta^T}{\partial t}\underline{I} = 0 \tag{35}$$

The vectors $\underline{w}$ are the kernels that give the fields at the plasma center from current sources. $\underline{w}_R$ refers to the vertical field, $\underline{w}_Z$ refers to the radial field, $\underline{w}_\kappa$ refers to the quadrupole field, and $\underline{w}_\delta$ refers to the hexapole field. The expressions containing the plasma parameters (such as Shafranov vertical field formula) have been moved to the left side of the equilibrium and velocity equations. Denoting zeroth order by "o" and first order by "1", and

expanding the dependent variables as the sum of zeroth and first order terms,

$$\underline{\underline{L}} = \underline{\underline{L}}_o + \underline{\underline{L}}_1 = \underline{\underline{L}}_o + \left.\frac{\partial \underline{\underline{L}}}{\partial R}\right|_o R_1 + \left.\frac{\partial \underline{\underline{L}}}{\partial Z}\right|_o Z_1 + \left.\frac{\partial \underline{\underline{L}}}{\partial \kappa}\right|_o \kappa_1 \tag{36}$$

$$\underline{\underline{R}} = \underline{\underline{R}}_o + \underline{\underline{R}}_1 = \underline{\underline{R}}_o + \left.\frac{\partial \underline{\underline{R}}}{\partial R}\right|_o R_1 + \left.\frac{\partial \underline{\underline{R}}}{\partial \kappa}\right|_o \kappa_1 \tag{37}$$

$$\underline{w}_R^T = \underline{w}_{R_o}^T + \left.\frac{\partial \underline{w}_R^T}{\partial R}\right|_o R_1 + \left.\frac{\partial \underline{w}_R^T}{\partial Z}\right|_o Z_1 + \left.\frac{\partial \underline{w}_R^T}{\partial \kappa}\right|_o \kappa_1 + \underline{I}_1^T \left.\frac{\partial \underline{w}_R}{\partial \underline{I}}\right|_o \tag{38}$$

$$\underline{w}_Z^T = \underline{w}_{Z_o}^T + \left.\frac{\partial \underline{w}_Z^T}{\partial R}\right|_o R_1 + \left.\frac{\partial \underline{w}_Z^T}{\partial Z}\right|_o Z_1 \tag{39}$$

$$\underline{w}_\kappa^T = \underline{w}_{\kappa_o}^T + \left.\frac{\partial \underline{w}_\kappa^T}{\partial R}\right|_o R_1 + \left.\frac{\partial \underline{w}_\kappa^T}{\partial Z}\right|_o Z_1 + \left.\frac{\partial \underline{w}_\kappa^T}{\partial \kappa}\right|_o \kappa_1 + \underline{I}_1^T \left.\frac{\partial \underline{w}_\kappa}{\partial \underline{I}}\right|_o \tag{40}$$

$$\begin{aligned}\underline{w}_\delta^T = {} & \underline{w}_{\delta_o}^T + \left.\frac{\partial \underline{w}_\delta^T}{\partial R}\right|_o R_1 + \left.\frac{\partial \underline{w}_\delta^T}{\partial Z}\right|_o Z_1 + \left.\frac{\partial \underline{w}_\delta^T}{\partial \kappa}\right|_o \kappa_1 \\ & + \left.\frac{\partial \underline{w}_\delta^T}{\partial \delta}\right|_o \delta_1 + \underline{I}_1^T \left.\frac{\partial \underline{w}_\delta^T}{\partial \underline{I}}\right|_o .\end{aligned} \tag{41}$$

Expanding the independent variables,

$$R = R_o + R_1 \qquad Z = Z_o + Z_1 \tag{42}$$

$$\kappa = \kappa_o + \kappa_1 \qquad \delta = \delta_o + \delta_1 \tag{43}$$

$$\underline{I} = \underline{I}_o + \underline{I}_1 \qquad \underline{V} = \underline{V}_o + \underline{V}_1 . \tag{44}$$

The linearized form of the vector circuit equation becomes,

$$\begin{aligned}&\underline{\underline{L}}_o \dot{\underline{I}}_1 + \left.\frac{\partial \underline{\underline{L}}}{\partial R}\right|_o \underline{I}_o \dot{R}_1 + \left.\frac{\partial \underline{\underline{L}}}{\partial Z}\right|_o \underline{I}_o \dot{Z}_1 + \left.\frac{\partial \underline{\underline{L}}}{\partial \kappa}\right|_o \underline{I}_o \dot{\kappa}_1 + \left(\left.\frac{\partial \underline{\underline{L}}}{\partial R}\right|_o \dot{\underline{I}}_o \right. \\ &+ \left.\frac{\partial^2 \underline{\underline{L}}}{\partial R^2}\right|_o \underline{I}_o \dot{R}_o + \left.\frac{\partial^2 \underline{\underline{L}}}{\partial Z \partial R}\right|_o \underline{I}_o \dot{Z}_o + \left.\frac{\partial^2 \underline{\underline{L}}}{\partial \kappa \partial R}\right|_o \underline{I}_o \dot{\kappa}_o + \left.\frac{\partial \underline{\underline{R}}}{\partial R}\right|_o \underline{I}_o \Big) R_1 \\ &+ \left(\left.\frac{\partial \underline{\underline{L}}}{\partial Z}\right|_o \dot{\underline{I}}_o + \left.\frac{\partial^2 \underline{\underline{L}}}{\partial R \partial Z}\right|_o \underline{I}_o \dot{R}_o + \left.\frac{\partial^2 \underline{\underline{L}}}{\partial Z^2}\right|_o \underline{I}_o \dot{Z}_o + \left.\frac{\partial^2 \underline{\underline{L}}}{\partial \kappa \partial Z}\right|_o \underline{I}_o \dot{\kappa} \right) Z_1 \\ &\left(\left.\frac{\partial \underline{\underline{L}}}{\partial \kappa}\right|_o \dot{\underline{I}}_o + \left.\frac{\partial^2 \underline{\underline{L}}}{\partial R \partial \kappa}\right|_o \underline{I}_o \dot{R}_o + \left.\frac{\partial^2 \underline{\underline{L}}}{\partial Z \partial \kappa}\right|_o \underline{I}_o \dot{Z}_o + \left.\frac{\partial^2 \underline{\underline{L}}}{\partial \kappa^2}\right|_o \underline{I}_o \dot{\kappa}_o \right.\end{aligned}$$

$$+\left.\frac{\partial \underline{\underline{R}}}{\partial \kappa}\right|_o \underline{I}_o\Bigg)\kappa_1+\Bigg(\left.\frac{\partial \underline{\underline{L}}}{\partial R}\right|_o \dot{R}_o+\left.\frac{\partial \underline{\underline{L}}}{\partial Z}\right|_o \dot{Z}_o+\left.\frac{\partial \underline{\underline{L}}}{\partial \kappa}\right|_o \dot{\kappa}_o+\underline{\underline{R}}_o+\frac{\partial \underline{\underline{L}}_o}{\partial t}\Bigg)\underline{I}_1=\underline{V}_1. \quad (45)$$

The equilibrium equations become

$$\left.\frac{\partial \underline{w}_R^T}{\partial R}\right|_o \underline{I}_o R_1+\left.\frac{\partial \underline{w}_R^T}{\partial Z}\right|_o \underline{I}_o Z_1+\left.\frac{\partial \underline{w}_R^T}{\partial \kappa}\right|_o \underline{I}_o\kappa_1+\underline{I}_1{}^T\left.\frac{\partial \underline{w}_R}{\partial \underline{I}}\right|_o \underline{I}_o+\underline{w}_{R_o}^T\underline{I}_1=0 \quad (46)$$

$$\left.\frac{\partial \underline{w}_Z^T}{\partial R}\right|_o \underline{I}_o R_1+\left.\frac{\partial \underline{w}_Z^T}{\partial Z}\right|_o \underline{I}_o Z_1+\underline{w}_{Z_o}^T\underline{I}_1=0 \quad (47)$$

$$\left.\frac{\partial \underline{w}_\kappa^T}{\partial R}\right|_o \underline{I}_o R_1+\left.\frac{\partial \underline{w}_\kappa^T}{\partial Z}\right|_o \underline{I}_o Z_1+\left.\frac{\partial \underline{w}_\kappa^T}{\partial \kappa}\right|_o \underline{I}_o\kappa_1+\underline{I}_1{}^T\left.\frac{\partial \underline{w}_\kappa}{\partial \underline{I}}\right|_o \underline{I}_o+\underline{w}_{\kappa_o}^T\underline{I}_1=0 \quad (48)$$

$$\left.\frac{\partial \underline{w}_\delta^T}{\partial R}\right|_o \underline{I}_o R_1+\left.\frac{\partial \underline{w}_\delta^T}{\partial Z}\right|_o \underline{I}_o Z_1+\left.\frac{\partial \underline{w}_\delta^T}{\partial \kappa}\right|_o \underline{I}_o\kappa_1+\left.\frac{\partial \underline{w}_\delta^T}{\partial \delta}\right|_o \underline{I}_o\delta_1+\underline{I}_1{}^T\left.\frac{\partial \underline{w}_\delta}{\partial \underline{I}}\right|_o \underline{I}_o+\underline{w}_{\delta_o}^T\underline{I}_1=0. \quad (49)$$

The linearized equation for the time derivative of the plasma major radius is,

$$\begin{aligned}
&\Bigg(\left.\frac{\partial^2 \underline{w}_R^T}{\partial R^2}\right|_o \underline{I}_o\dot{R}_o+\left.\frac{\partial^2 \underline{w}_R^T}{\partial Z\partial R}\right|_o \underline{I}_o\dot{Z}_o+\left.\frac{\partial^2 \underline{w}_R^T}{\partial \kappa\partial R}\right|_o \underline{I}_o\dot{\kappa}_o+\dot{\underline{I}}_o{}^T\left.\frac{\partial^2 \underline{w}_R}{\partial \underline{I}\partial R}\right|_o \underline{I}_o\\
&+\left.\frac{\partial \underline{w}_R^T}{\partial R}\right|_o \dot{\underline{I}}_o+\left.\frac{\partial^2 \underline{w}_R^T}{\partial \beta_p\partial R}\right|_o \underline{I}_o\dot{\beta}_p+\left.\frac{\partial^2 \underline{w}_R^T}{\partial \frac{l_i}{2}\partial R}\right|_o \underline{I}_o\frac{\dot{l}_i}{2}\Bigg)R_1+\Bigg(\left.\frac{\partial^2 \underline{w}_R^T}{\partial R\partial Z}\right|_o \underline{I}_o\dot{R}_o\\
&+\left.\frac{\partial^2 \underline{w}_R^T}{\partial Z^2}\right|_o \underline{I}_o\dot{Z}_o+\left.\frac{\partial \underline{w}_R^T}{\partial Z}\right|_o \dot{\underline{I}}_o\Bigg)Z_1+\Bigg(\left.\frac{\partial^2 \underline{w}_R^T}{\partial R\partial \kappa}\right|_o \underline{I}_o\dot{R}_o+\left.\frac{\partial^2 \underline{w}_R^T}{\partial \kappa^2}\right|_o \underline{I}_o\dot{\kappa}_o\\
&\dot{\underline{I}}_o{}^T\left.\frac{\partial^2 \underline{w}_R}{\partial \underline{I}\partial \kappa}\right|_o \underline{I}_o+\left.\frac{\partial \underline{w}_R^T}{\partial \kappa}\right|_o \dot{\underline{I}}_o+\left.\frac{\partial^2 \underline{w}_R^T}{\partial \beta_p\partial \kappa}\right|_o \underline{I}_o\dot{\beta}_p+\left.\frac{\partial^2 \underline{w}_R^T}{\partial \frac{l_i}{2}\partial \kappa}\right|_o \underline{I}_o\frac{\dot{l}_i}{2}\Bigg)\kappa_1\\
&+\left.\frac{\partial \underline{w}_R^T}{\partial R}\right|_o \underline{I}_o\dot{R}_1+\left.\frac{\partial \underline{w}_R^T}{\partial Z}\right|_o \underline{I}_o\dot{Z}_1+\left.\frac{\partial \underline{w}_R^T}{\partial \kappa}\right|_o \underline{I}_o\dot{\kappa}_1+\underline{I}_1{}^T\Bigg(\left.\frac{\partial^2 \underline{w}_R}{\partial R\partial \underline{I}}\right|_o \underline{I}_o\dot{R}_o\\
&+\left.\frac{\partial^2 \underline{w}_{,l}}{\partial \kappa\partial \underline{I}}\right|_o \underline{I}_o\dot{\kappa}_o+\left.\frac{\partial \underline{w}_R}{\partial \underline{I}}\right|_o \dot{\underline{I}}_o+\left.\frac{\partial^2 \underline{w}_R}{\partial \beta_p\partial \underline{I}}\right|_o \underline{I}_o\dot{\beta}_p+\left.\frac{\partial^2 \underline{w}_R}{\partial \underline{I}\partial \underline{I}}\right|_o \underline{I}_o\dot{\underline{I}}_o\Bigg)\\
&+\Bigg(\left.\frac{\partial \underline{w}_R^T}{\partial R}\right|_o \dot{R}_o+\left.\frac{\partial \underline{w}_R^T}{\partial Z}\right|_o \dot{Z}_o+\left.\frac{\partial \underline{w}_R^T}{\partial \kappa}\right|_o \dot{\kappa}_o+\dot{\underline{I}}_o{}^T\left.\frac{\partial \underline{w}_R}{\partial \underline{I}}\right|_o
\end{aligned}$$

$$+ \left.\frac{\partial \underline{w}_R^T}{\partial \beta_p}\right|_o \dot{\beta}_p + \left.\frac{\partial \underline{w}_R^T}{\partial \frac{l_i}{2}}\right|_o \frac{\dot{l}_i}{2}\Bigg) \underline{I}_1 + \dot{\underline{I}}_1^T \left.\frac{\partial \underline{w}_R}{\partial \underline{I}}\right|_o \underline{I}_o + \underline{w}_{R_o}^T \dot{\underline{I}}_1 = 0. \qquad (50)$$

The linearized equation for the time derivative of the plasma vertical position is,

$$\Bigg(\left.\frac{\partial^2 \underline{w}_Z^T}{\partial R^2}\right|_o \underline{I}_o \dot{R}_o + \left.\frac{\partial^2 \underline{w}_Z^T}{\partial Z \partial R}\right|_o \underline{I}_o \dot{Z}_o + \left.\frac{\partial \underline{w}_Z^T}{\partial R}\right|_o \dot{\underline{I}}_o\Bigg) R_1 + \Bigg(\left.\frac{\partial^2 \underline{w}_Z^T}{\partial R \partial Z}\right|_o \underline{I}_o \dot{R}_o$$
$$+ \left.\frac{\partial^2 \underline{w}_Z^T}{\partial Z^2}\right|_o \underline{I}_o \dot{Z}_o + \left.\frac{\partial \underline{w}_Z^T}{\partial Z}\right|_o \dot{\underline{I}}_o\Bigg) Z_1 + \left.\frac{\partial \underline{w}_Z^T}{\partial R}\right|_o \underline{I}_o \dot{R}_1 + \left.\frac{\partial \underline{w}_Z^T}{\partial Z}\right|_o \underline{I}_o \dot{Z}_1$$
$$+ \Bigg(\left.\frac{\partial \underline{w}_Z^T}{\partial R}\right|_o \dot{R}_o + \left.\frac{\partial \underline{w}_Z^T}{\partial Z}\right|_o \dot{Z}_o\Bigg) \underline{I}_1 + \underline{w}_{Z_o}^T \dot{\underline{I}}_1 = 0. \qquad (51)$$

The linearized equation for the time derivative of the plasma elongation is,

$$\Bigg(\left.\frac{\partial^2 \underline{w}_\kappa^T}{\partial R^2}\right|_o \underline{I}_o \dot{R}_o + \left.\frac{\partial^2 \underline{w}_\kappa^T}{\partial Z \partial R}\right|_o \underline{I}_o \dot{Z}_o + \left.\frac{\partial^2 \underline{w}_\kappa^T}{\partial \kappa \partial R}\right|_o \underline{I}_o \dot{\kappa}_o + \dot{\underline{I}}_o^T \left.\frac{\partial^2 \underline{w}_\kappa}{\partial \underline{I} \partial R}\right|_o \underline{I}_o$$
$$+ \left.\frac{\partial \underline{w}_\kappa^T}{\partial R}\right|_o \dot{\underline{I}}_o + \left.\frac{\partial^2 \underline{w}_\kappa^T}{\partial \beta_p \partial R}\right|_o \underline{I}_o \dot{\beta}_p\Bigg) R_1 + \Bigg(\left.\frac{\partial^2 \underline{w}_\kappa^T}{\partial R \partial Z}\right|_o \underline{I}_o \dot{R}_o + \left.\frac{\partial^2 \underline{w}_\kappa^T}{\partial Z^2}\right|_o \underline{I}_o \dot{Z}_o$$
$$+ \left.\frac{\partial \underline{w}_\kappa^T}{\partial Z}\right|_o \dot{\underline{I}}_o\Bigg) Z_1 + \Bigg(\left.\frac{\partial^2 \underline{w}_\kappa^T}{\partial R \partial \kappa}\right|_o \underline{I}_o \dot{R}_o + \left.\frac{\partial^2 \underline{w}_\kappa^T}{\partial \kappa^2}\right|_o \dot{\underline{I}}_o^T \left.\frac{\partial^2 \underline{w}_\kappa}{\partial \underline{I} \partial \kappa}\right|_o \underline{I}_o$$
$$+ \left.\frac{\partial \underline{w}_\kappa^T}{\partial \kappa}\right|_o \dot{\underline{I}}_o + \left.\frac{\partial^2 \underline{w}_\kappa^T}{\partial \beta_p \partial \kappa}\right|_o \underline{I}_o \dot{\beta}_p\Bigg) \kappa_1 + \left.\frac{\partial \underline{w}_\kappa^T}{\partial R}\right|_o \underline{I}_o \dot{R}_1 + \left.\frac{\partial \underline{w}_\kappa^T}{\partial Z}\right|_o \underline{I}_o \dot{Z}_1$$
$$+ \left.\frac{\partial \underline{w}_\kappa^T}{\partial \kappa}\right|_o \underline{I}_o \dot{\kappa}_1 + \underline{I}_1^T \Bigg(\left.\frac{\partial^2 \underline{w}_\kappa}{\partial R \partial \underline{I}}\right|_o \underline{I}_o \dot{R}_o + \left.\frac{\partial^2 \underline{w}_\kappa}{\partial \kappa \partial \underline{I}}\right|_o \underline{I}_o \dot{\kappa}_o + \left.\frac{\partial^2 \underline{w}_\kappa}{\partial \underline{I} \partial \underline{I}}\right|_o \underline{I}_o \dot{\underline{I}}_o$$
$$+ \left.\frac{\partial \underline{w}_\kappa}{\partial \underline{I}}\right|_o \dot{\underline{I}}_o + \left.\frac{\partial^2 \underline{w}_\kappa}{\partial \beta_p \partial \underline{I}}\right|_o \underline{I}_o \dot{\beta}_p\Bigg) + \Bigg(\left.\frac{\partial \underline{w}_\kappa^T}{\partial R}\right|_o \dot{R}_o + \left.\frac{\partial \underline{w}_\kappa^T}{\partial Z}\right|_o \dot{Z}_o$$
$$+ \left.\frac{\partial \underline{w}_\kappa^T}{\partial \kappa}\right|_o \dot{\kappa}_o + \dot{\underline{I}}_o^T \left.\frac{\partial \underline{w}_\kappa}{\partial \underline{I}}\right|_o + \left.\frac{\partial \underline{w}_\kappa^T}{\partial \beta_p}\right|_o \dot{\beta}_p\Bigg) \underline{I}_1 + \underline{w}_{\kappa_o}^T \dot{\underline{I}}_1 + \dot{\underline{I}}_1^T \left.\frac{\partial \underline{w}_\kappa}{\partial \underline{I}}\right|_o \underline{I}_o = 0. \qquad (52)$$

The linearized equation for the time derivative of the plasma triangularity is,

$$
\left(\left. \frac{\partial^2 \underline{w}_\delta^T}{\partial R^2} \right|_o \underline{I}_o \dot{R}_o + \left. \frac{\partial^2 \underline{w}_\delta^T}{\partial Z \partial R} \right|_o \underline{I}_o \dot{Z}_o + \left. \frac{\partial^2 \underline{w}_\delta^T}{\partial \kappa \partial R} \right|_o \underline{I}_o \dot{\kappa}_o + \left. \frac{\partial^2 \underline{w}_\delta^T}{\partial \delta \partial R} \right|_o \underline{I}_o \dot{\delta}_o \right.
$$

$$
+ \underline{\dot{I}}_o^T \left. \frac{\partial^2 \underline{w}_\delta}{\partial \underline{I} \partial R} \right|_o \underline{I}_o + \left. \frac{\partial \underline{w}_\delta^T}{\partial R} \right|_o \underline{\dot{I}}_o + \left. \frac{\partial^2 \underline{w}_\delta^T}{\partial \beta_p \partial R} \right|_o \underline{I}_o \dot{\beta}_p \Bigg) R_1 + \left(\left. \frac{\partial^2 \underline{w}_\delta^T}{\partial R \partial Z} \right|_o \underline{I}_o \dot{R}_o \right.
$$

$$
+ \left. \frac{\partial^2 \underline{w}_\delta^T}{\partial Z^2} \right|_o \underline{I}_o \dot{Z}_o + \left. \frac{\partial \underline{w}_\delta^T}{\partial Z} \right|_o \underline{\dot{I}}_o \Bigg) Z_1 + \left(\left. \frac{\partial^2 \underline{w}_\delta^T}{\partial R \partial \kappa} \right|_o \underline{I}_o \dot{R}_o + \left. \frac{\partial^2 \underline{w}_\delta^T}{\partial \kappa^2} \right|_o \underline{I}_o \dot{\kappa}_o \right.
$$

$$
+ \left. \frac{\partial^2 \underline{w}_\delta^T}{\partial \delta \partial \kappa} \right|_o \underline{I}_o \dot{\delta}_o + \underline{\dot{I}}_o^T \left. \frac{\partial^2 \underline{w}_\delta}{\partial \underline{I} \partial \kappa} \right|_o \underline{I}_o + \left. \frac{\partial \underline{w}_\delta^T}{\partial \kappa} \right|_o \underline{\dot{I}}_o + \left. \frac{\partial^2 \underline{w}_\delta^T}{\partial \beta_p \partial \kappa} \right|_o \underline{I}_o \dot{\beta}_p \Bigg) \kappa_1
$$

$$
+ \left(\left. \frac{\partial^2 \underline{w}_\delta^T}{\partial R \partial \delta} \right|_o \underline{I}_o \dot{R}_o + \left. \frac{\partial^2 \underline{w}_\delta^T}{\partial \kappa \partial \delta} \right|_o \underline{I}_o \dot{\kappa}_o + \underline{\dot{I}}_o^T \left. \frac{\partial^2 \underline{w}_\delta}{\partial \underline{I} \partial \delta} \right|_o \underline{I}_o + \left. \frac{\partial \underline{w}_\delta^T}{\partial \delta} \right|_o \underline{\dot{I}}_o \right.
$$

$$
+ \left. \frac{\partial^2 \underline{w}_\delta^T}{\partial \beta_p \partial \delta} \right|_o \underline{I}_o \dot{\beta}_p \Bigg) \delta_1 + \left. \frac{\partial \underline{w}_\delta^T}{\partial R} \right|_o \underline{I}_o \dot{R}_1 + \left. \frac{\partial \underline{w}_\delta^T}{\partial Z} \right|_o \underline{I}_o \dot{Z}_1 + \left. \frac{\partial \underline{w}_\delta^T}{\partial \kappa} \right|_o \underline{I}_o \dot{\kappa}_1
$$

$$
+ \left. \frac{\partial \underline{w}_\delta^T}{\partial \delta} \right|_o \underline{I}_o \dot{\delta}_1 + \underline{I}_1^T \left(\left. \frac{\partial^2 \underline{w}_\delta}{\partial R \partial \underline{I}} \right|_o \underline{I}_o \dot{R}_o + \left. \frac{\partial^2 \underline{w}_\delta}{\partial \kappa \partial \underline{I}} \right|_o \underline{I}_o \dot{\kappa}_o + \left. \frac{\partial \underline{w}_\delta}{\partial \delta \partial \underline{I}} \right|_o \underline{I}_o \dot{\delta}_o \right.
$$

$$
+ \left. \frac{\partial \underline{w}_\delta}{\partial \underline{I}} \right|_o \underline{\dot{I}}_o + \left. \frac{\partial^2 \underline{w}_\delta}{\partial \beta_p \partial \underline{I}} \right|_o \underline{I}_o \dot{\beta}_p \Bigg) + \left(\left. \frac{\partial \underline{w}_\delta^T}{\partial R} \right|_o \dot{R}_o + \left. \frac{\partial \underline{w}_\delta^T}{\partial Z} \right|_o \dot{Z}_o \right.
$$

$$
+ \left. \frac{\partial \underline{w}_\delta^T}{\partial \kappa} \right|_o \dot{\kappa}_o + \left. \frac{\partial \underline{w}_\delta^T}{\partial \delta} \right|_o \dot{\delta}_o + \underline{\dot{I}}_o^T \left. \frac{\partial^2 \underline{w}_\delta}{\partial \underline{I} \partial \underline{I}} \right|_o \underline{I}_o + \underline{\dot{I}}_o^T \left. \frac{\partial \underline{w}_\delta}{\partial \underline{I}} \right|_o
$$

$$
+ \left. \frac{\partial \underline{w}_\delta^T}{\partial \beta_p} \right|_o \dot{\beta}_p \Bigg) \underline{I}_1 + \underline{w}_{\delta_o}^T \underline{\dot{I}}_1 + \underline{\dot{I}}_1^T \left. \frac{\partial \underline{w}_\delta}{\partial \underline{I}} \right|_o \underline{I}_o = 0. \tag{53}
$$

These equations are more conveniently expressed in matrix form. The circuit equation contains terms that must be eliminated by substitution of the equilibrium and velocity equations. The vector $\underline{Z}$ will be defined as $[R, Z, \kappa]$. The circuit, equilibrium, and velocity equations are shown, respectively.

$$
\underline{\underline{E}} \dot{\underline{I}}_1 + \underline{\underline{F}} \underline{I}_1 + \underline{\underline{G}} \dot{\underline{Z}}_1 + \underline{\underline{H}} \underline{Z}_1 = \underline{\underline{I}}_{nn} \underline{V}_1 \tag{54}
$$

$$
\underline{\underline{U}} \underline{Z}_1 = -\underline{\underline{V}} \underline{I}_1 \tag{55}
$$

$$
\underline{\underline{P}} \dot{\underline{Z}}_1 = -\underline{\underline{Q}} \underline{Z}_1 - \underline{\underline{S}} \underline{I}_1 - \underline{\underline{T}} \dot{\underline{I}}_1 \tag{56}
$$

The matrix $\underline{\underline{I_{nm}}}$ refers to a rectangular matrix with ones on its diagonal, with n the number of currents and m the number of voltages. After substituting into the vector circuit equation to give an equation depending only on the currents and voltages, the definitions of $\underline{\underline{A}}$ and $\underline{\underline{B}}$ are,

$$\underline{\underline{A}} = -\left[\underline{\underline{E}} - \underline{\underline{GP}}^{-1}\underline{\underline{T}}\right]^{-1}\left[\underline{\underline{GP}}^{-1}\underline{\underline{QU}}^{-1}\underline{\underline{V}} - \underline{\underline{GP}}^{-1}\underline{\underline{S}} - \underline{\underline{HU}}^{-1}\underline{\underline{V}} + \underline{\underline{F}}\right] \quad (57)$$

$$\underline{\underline{B}} = \left[\underline{\underline{E}} - \underline{\underline{GP}}^{-1}\underline{\underline{T}}\right]^{-1}\underline{\underline{I_{nm}}}. \quad (58)$$

In addition, are the relations between the parameters to be controlled and the currents in the system. A vector relation for these can be given by,

$$\underline{\underline{W}}\underline{Y}_1 = \underline{\underline{X}}\underline{I}_1. \quad (59)$$

The matrix $\underline{\underline{C}}$ is defined as $\underline{\underline{W}}^{-1}\underline{\underline{X}}$. It was necessary to use an algebraic manipulator algorithm call REDUCE to generate the high order derivatives for the field quantities and the linearization in cases of complicated dependences.

B Optimization

In order to generate an optimal control a function representing the system performance must be created, to specify what the objective of the control is. The objective of the control is to find the correction to the nominal voltages on the coils that keep perturbations in the controlled variables $[R, Z, \kappa, \delta, I_p]$ near zero, and spend as little effort as possible in doing so. The time dependence of terms will be suppressed in the following. A function that represents this objective is,

$$J = \int_0^T \left[\underline{Y}_1^T\underline{\underline{Q}}\underline{Y}_1 + \underline{V}_1^T\underline{\underline{R}}\underline{V}_1\right] dt. \quad (60)$$

We want to minimize this integral over time. However, the system behaves according to specific dynamics and so these must be incorporated when deriving the optimal control. This is done by constraining the optimization to obey the linear dynamics equations,

$$\dot{\underline{I}}_1 = \underline{\underline{A}}\underline{I}_1 + \underline{\underline{B}}\underline{V}_1 \quad (61)$$

$$\underline{Y}_1 = \underline{\underline{C}}\underline{I}_1. \quad (62)$$

We will not constrain the values that the I_1's and V_1's can take. One of the more straightforward ways to minimize a functional with constraints is by creating a Hamiltonian for the problem.

$$H = \underline{I}_1^T \underline{\underline{C}}^T \underline{\underline{Q}} \underline{\underline{C}} \underline{I}_1 + \underline{V}_1^T \underline{\underline{R}} \underline{V}_1 + \underline{\lambda}^T \left[\underline{\underline{A}} \underline{I}_1 + \underline{\underline{B}} \underline{V}_1 \right] \tag{63}$$

Here $\underline{\lambda}$ represents a vector of Lagrange multipliers. The necessary conditions for optimality, which can be found elsewhere[27], are,

$$-\frac{\partial H}{\partial \underline{I}_1} = \dot{\underline{\lambda}}^T \tag{64}$$

$$\frac{\partial H}{\partial \underline{V}_1} = 0 \tag{65}$$

$$\frac{\partial H}{\partial \underline{\lambda}^T} = \dot{\underline{I}}_1 \tag{66}$$

$$\underline{\lambda}(T) = \underline{\underline{P}}(T) \underline{I}_1(T). \tag{67}$$

The third condition only returns our linear dynamics equations, and the last is a boundary condition at the final time. The first two yield,

$$\underline{V}_1 = -\underline{\underline{R}}^{-1} \underline{\underline{B}}^T \underline{\lambda} \tag{68}$$

$$\dot{\underline{\lambda}} = -\underline{\underline{C}}^T \underline{\underline{Q}} \underline{\underline{C}} \underline{I}_1 - \underline{\underline{A}}^T \underline{\lambda}. \tag{69}$$

Using the boundary conditions and the above derived equations, it can be shown[24] that the vector of Lagrange multipliers is linearly related to the currents for all time.

$$\underline{\lambda} = \underline{\underline{P}} \underline{I}_1 \tag{70}$$

Using this, the optimal control vector $\underline{V}_1$ is a linear function of the currents in the system.

$$\underline{V}_1 = -\underline{\underline{R}}^{-1} \underline{\underline{B}}^T \underline{\underline{P}} \underline{I}_1 \tag{71}$$

The equation satisfied by the matrix $\underline{\underline{P}}$ can be derived by substituting $\underline{\lambda} = \underline{\underline{P}} \underline{I}_1$ into the equation for $\dot{\underline{\lambda}}$ and using the linear dynamics equation.

$$\underline{\underline{P}} \underline{\underline{A}} + \underline{\underline{A}}^T \underline{\underline{P}} - \underline{\underline{P}} \underline{\underline{B}} \underline{\underline{R}}^{-1} \underline{\underline{B}}^T \underline{\underline{P}} + \underline{\underline{C}}^T \underline{\underline{Q}} \underline{\underline{C}} = -\dot{\underline{\underline{P}}} \tag{72}$$

In the present work only the steady-state solution for $\underline{\underline{P}}$ is sought, so the upper limit in the cost functional integral is made infinite, and the equation satisfied by the matrix is the nonlinear algebraic matrix equation given by the above with $-\underline{\underline{\dot{P}}}$ set to zero. Rather than actually using the matrix equation to solve for the Riccati matrix, the differential system is typically used.

$$\begin{bmatrix} \dot{\underline{I}}_1 \\ \dot{\underline{\lambda}}_1 \end{bmatrix} = \begin{bmatrix} \underline{\underline{A}} & -\underline{\underline{B}}\underline{\underline{R}}^{-1}\underline{\underline{B}}^T \\ -\underline{\underline{Q}} & -\underline{\underline{A}}^T \end{bmatrix} = \begin{bmatrix} \underline{I}_1 \\ \underline{\lambda} \end{bmatrix} \tag{73}$$

The steady-state Riccati matrix can be found by diagonalizing the above system matrix and using the eigenvectors[24].

C Modal Reduction

The basic idea behind reduction of order is to construct a reduced description of the system that still contains all the important behavior, use this model to construct an optimal control law, and then apply the resulting control law to the original larger system. For the control to be useful it should stabilize the system and hopefully give acceptable responses to perturbations to the system. The method used here is a modal reduction, also called aggregation. In the method the reduced order state variables are linearly related to the original system state variables (in a tokamak these are the currents). The time dependence of terms will be suppressed in the following. The original and reduced systems are given by,

$$\dot{\underline{I}}_1 = \underline{\underline{A}}\underline{I}_1 + \underline{\underline{B}}\underline{V}_1 \qquad \dot{\underline{z}} = \underline{\underline{F}}\underline{z} + \underline{\underline{G}}\underline{V}_1 \tag{74}$$

$$\underline{z} = \underline{\underline{H}}\underline{I}_1 \qquad \underline{\underline{F}} = \underline{\underline{H}}\underline{\underline{A}}\underline{\underline{H}}^T(\underline{\underline{H}}\underline{\underline{H}}^T)^{-1} \qquad \underline{\underline{G}} = \underline{\underline{H}}\underline{\underline{B}}. \tag{75}$$

Here $\dim(\underline{z})$ is less than $\dim(\underline{I}_1)$. Once the matrix $\underline{\underline{H}}$ is chosen, a new cost functional is created that weights the states of the reduced system and the same voltages as the original system (a system would not be reduced below the number of coils). The control derived is the optimal control for the reduced system.

$$J_z = \int_0^T \left[\underline{z}^T\underline{\underline{Q}}_z\underline{z} + \underline{V}_1^T\underline{\underline{R}}\underline{V}_1\right] dt \tag{76}$$

$$\underline{\underline{Q}}_z = (\underline{\underline{H}}\underline{\underline{H}}^T)^{-1}\underline{\underline{H}}\underline{\underline{C}}^T\underline{\underline{Q}}\underline{\underline{C}}\underline{\underline{H}}^T(\underline{\underline{H}}\underline{\underline{H}}^T)^{-1} \tag{77}$$

$$\underline{V}_1 = -\underline{\underline{R}}^{-1}\underline{\underline{G}}^T\underline{\underline{P}}_r\underline{z} \tag{78}$$

The matrix $\underline{\underline{P}}_r$ is the Riccati matrix for the reduced system. This modal approach involves preserving dominant eigenvalues, and any positive or near zero eigenvalues, of the original system in the reduced order model. The large negative eigenvalues corresponding to quickly damped behavior are neglected. The original system is diagonalized to yield the eigenvalues and eigenvectors.

$$\dot{\underline{y}} = \underline{\underline{\Lambda}}\underline{y} + \underline{\underline{\Gamma}}\underline{V}_1 \qquad \underline{I}_1 = \underline{\underline{M}}\underline{y} \tag{79}$$

$\underline{\underline{\Lambda}}$ is the diagonal matrix of eigenvalues of the original system matrix $\underline{\underline{A}}$ and is defined as $\underline{\underline{\Lambda}} = \underline{\underline{M}}^{-1}\underline{\underline{A}}\underline{\underline{M}}$. The modal matrix is taken and all columns corresponding to nondominant eigenvalues are removed. Then all rows corresponding to nondominant eigenvectors are removed, yeilding a square reduced modal matrix. From these series of linear transformations the matrix $\underline{\underline{H}}$ can be derived. The eigenvalues of the matrix $\underline{\underline{F}}$ will be exactly those eigenvalues of the original matrix $\underline{\underline{A}}$ that were retained in the reduced model. When the optimal control law calculated for the reduced order model is applied to the original system, the resulting closed loop eigenvalues will be those of the closed loop reduced system and those remaining nondominant eigenvalues of the original system matrix $\underline{\underline{A}}$. This results in a suboptimal control relative to the control derived for the original system, feeding back all the currents in the system. These modal states do not necessarily correspond directly to currents in the original system, but are linear combinations of them.

Acknowledgements

This work was supported by the U.S. Department of Energy, while at UCLA under contract Nos. DE-FG03-80ER52061 and DE-FG03-86ER52126, and at PPPL under contract No. DE-AC02-76CH03073.

References

[1] ARTEMENKOV, L. I., GOLOVIN, I. N., KOZLOV, P. I., et al., Nuclear Fusion 12 Supplement (1972) 27.

[2] HUGILL, J., GIBSON, A., Nuclear Fusion 14 (1974) 611.

[3] ANDERSON, J. L., BOOTH, R. S., COLCHIN, R. J., MISKELL, R. V., BAILEY, J. M., Nuclear Fusion 16 (1976) 629.

[4] FUGIWARA, M., ITOH, S., MATSUOKA, K., MASUURA, K., MIYAMOTO, K., OGATA, A., Japanese Journal of Applied Physics 14 (1975) 675.

[5] NOLL, P., AIGLE, R., BROWNE, M. L., et al., Symposium on Fusion Engineering (11^{th}, Austin, Texas, 1985), Vol.1, IEEE, New York (1986) 33.

[6] KONDO, I., KIMURA, T., YONEKAWA, I., et al., Fusion Engineering and Design 5 (1987) 69.

[7] KALNAVARNS, J., PACHER, G. W., PACHER, H. D., Symposium on Fusion Engineering (11^{th}, Austin, Texas, 1985), Vol.1, IEEE, New York (1986) 389.

[8] NEILSON, G. H., DYER, G. R., EDMONDS, P. H., Nuclear Fusion 24 (1984) 1291.

[9] LAZARUS, E. A., NEILSON, G. H., Nuclear Fusion 27 (1987) 383.

[10] NAGAYAMA, Y., NAITO, N., UEDA, Y., OHKI, Y., MIYAMOTO, K., Nuclear Fusion 24 (1984) 1242.

[11] KIKUCHI, M., NINOMIYA, H., YOSHINO, R., SEKI, S., Nuclear Fusion 27 (1987) 299.

[12] MORI, M., SUZUKI, N., SHOJI, T., YANAGISAWA, I., TANI, T., MATSUZAKI, Y., Nuclear Fusion 27 (1987) 725.

[13] YOUNG, K. M., BELL, M., BLANCHARD, W. R., et al., Plasma Physics and Controlled Fusion 26 (1984) 11.

[14] GRAN, R., ROSSI, M., SOBIERAJSKI, F., Symposium on Engineering Problems of Fusion Research (7^{th}, Knoxville, Tn., 1977), Vol.1, IEEE, New York (1983) 1233.

[15] GRAN, R., ROSSI, M., FIRESTONE, M., Symposium on Engineering Problems of Fusion Research (8^{th}, San Francisco, Ca., 1979), Vol.4, IEEE, New York (1979) 1854.

[16] FIRESTONE, M., IEEE Transactions on Plasma Science PS- 10 (1982) 105.

[17] OGATA, A., NINOMIYA, H., Japanese Journal of Applied Physics 18 (1979) 825.

[18] OGATA, A., NINOMIYA, H., Symposium on Engineering Problems of Fusion Research (8^{th}, San Francisco, Ca., 1979), Vol.4, IEEE, New York (1979) 1879.

[19] JT-60 TEAM, Plasma Physics and Controlled Fusion 28 (1986) 165.

[20] U.S. FED-INTOR and U.S. Contribution to the INTOR Phase 2A Workshop, Oct. 1982.

[21] BROWN, D. I., BELL, M. G., COONROD, J., Symposium on Fusion Engineering (10^{th}, Philadelphia, Pa., 1983), Vol.2, IEEE, New York (1983) 1233.

[22] KESSEL, C. E., FIRESTONE, M. A., Fusion Technology 10 (1986) 1177.

[23] STRICKLER, D. J., MILLER, J. B., ROTHE, K. E., PENG, Y.-K. M., Equilibrium Modeling of the TFCX Poloidal Field Coil System, ORNL/FEDC-83/10, Oak Ridge National Laboratory, Oak Ridge (1984).

[24] KWAKERNAAK, H., SIVAN, R., Linear Optimal Control Systems, Wiley-Interscience, New York (1972).

[25] FORTMANN, T. E., HITZ, K. L., An Introduction to Linear Control Systems, Marcel Dekker Inc., New York (1977).

[26] ANDERSON, B. D. O., MOORE, J. B., Linear Optimal Control, Prentice-Hall Inc., New Jersey (1971).

[27] ELBERT, T. F., Estimation and Control of Systems, Van Nostrand Reinhold Co., New York (1984).

[28] KESSEL, C. E., Linear Optimal Control of Plasma Position, Shape, and Current in a Tokamak Fusion Reactor, Ph.D. Dissertation, University of California, Los Angeles, 1987.

Table 1: Equilibrium trajectory of various parameters

time(sec)	$I_p(MA)$	R(m)	Z(mm)	a(m)	κ	δ	β_p
0.30	0.40	5.32	3.10	1.20	1.10	-0.006	0.01
0.48	0.64	5.32	1.00	1.20	1.10	-0.006	0.02
0.65	0.87	5.32	-1.00	1.20	1.10	-0.006	0.03
0.83	1.10	5.32	-2.00	1.20	1.10	-0.006	0.04
1.00	1.31	5.32	-1.00	1.20	1.10	-0.006	0.05
1.50	1.91	5.35	6.50	1.20	1.15	0.014	0.08
2.25	2.75	5.36	9.20	1.20	1.22	0.047	0.20
3.00	3.51	5.37	8.30	1.20	1.29	0.080	0.50
4.50	4.86	5.36	5.20	1.20	1.42	0.130	0.97
6.00	6.00	5.31	9.40	1.20	1.57	0.166	1.95

List of Figures

Figure 11. Voltage on outermost PF coil as a function of time for discrete control with sampling times of 1 ms. (solid), 10 ms. (dash), and 20 ms. (dot).

Figure 12. Plasma major radius as a function of time for comparison of full order (dash) and reduced models of order 13 (a), 15 (b), and 20 (c) (solid).

Figure 13. Plasma elongation as a function of time for comparison of full order (dash) and reduced models of order 13 (a), 15 (b), and 20 (c) (solid).

#89X0221

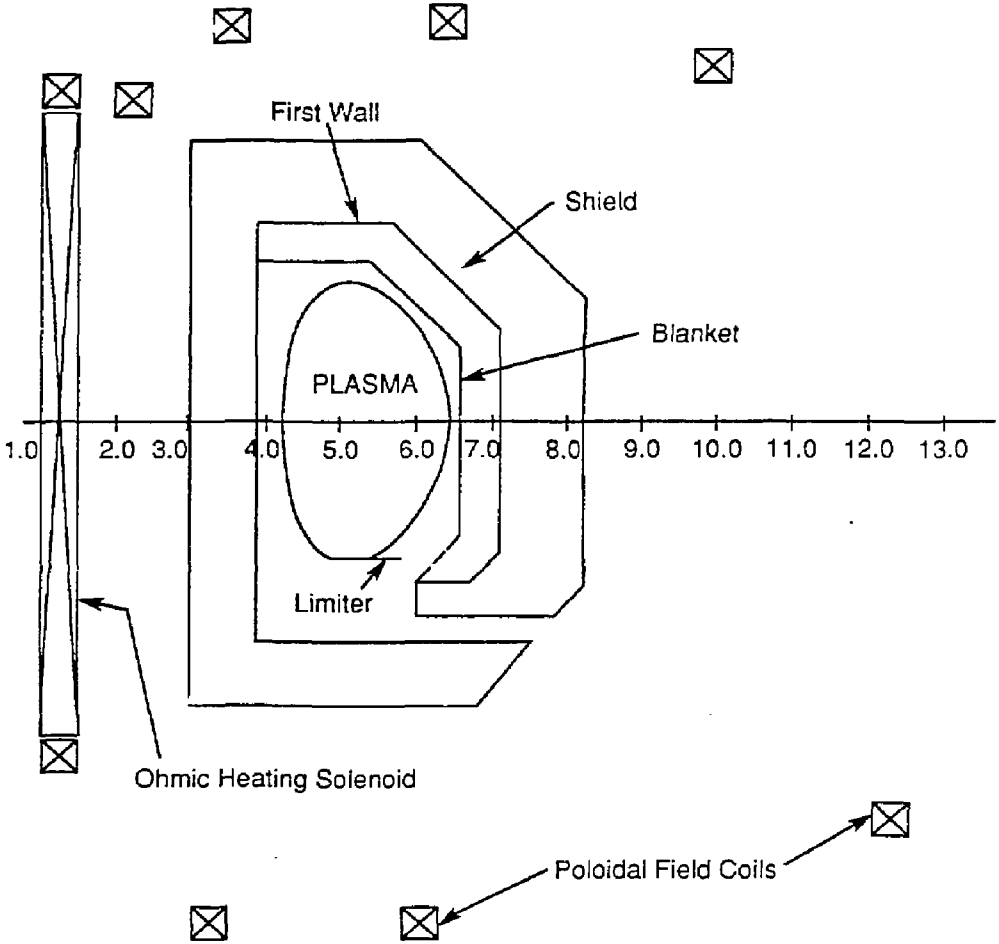

Fig. 1

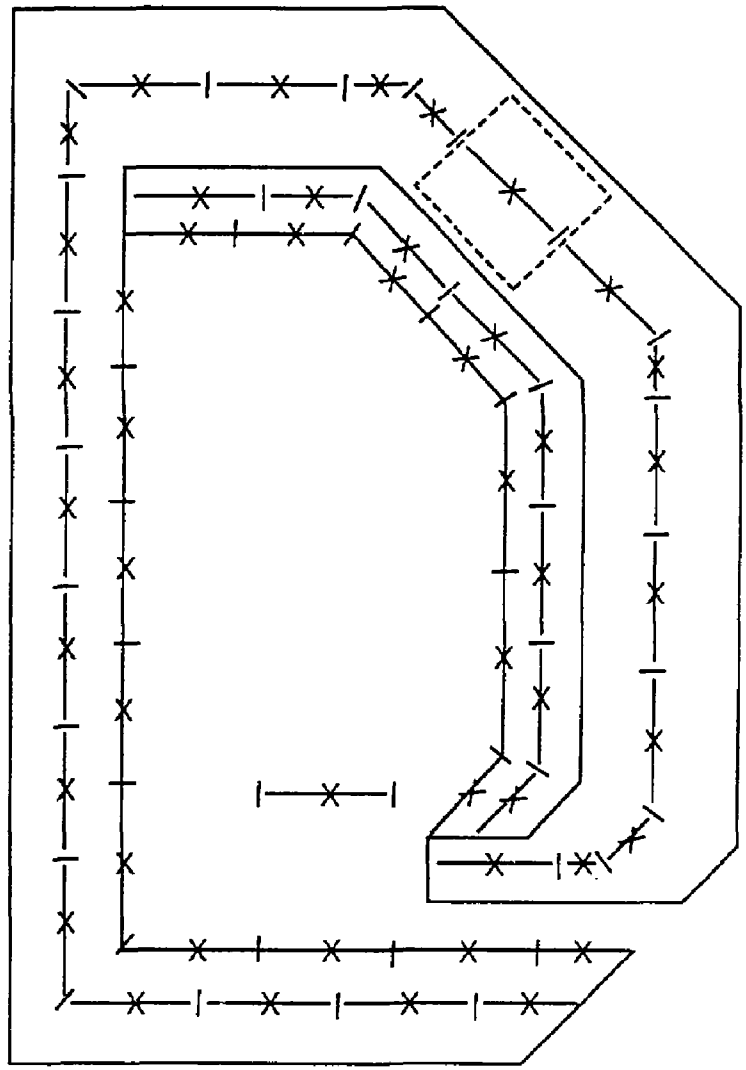

Fig. 2

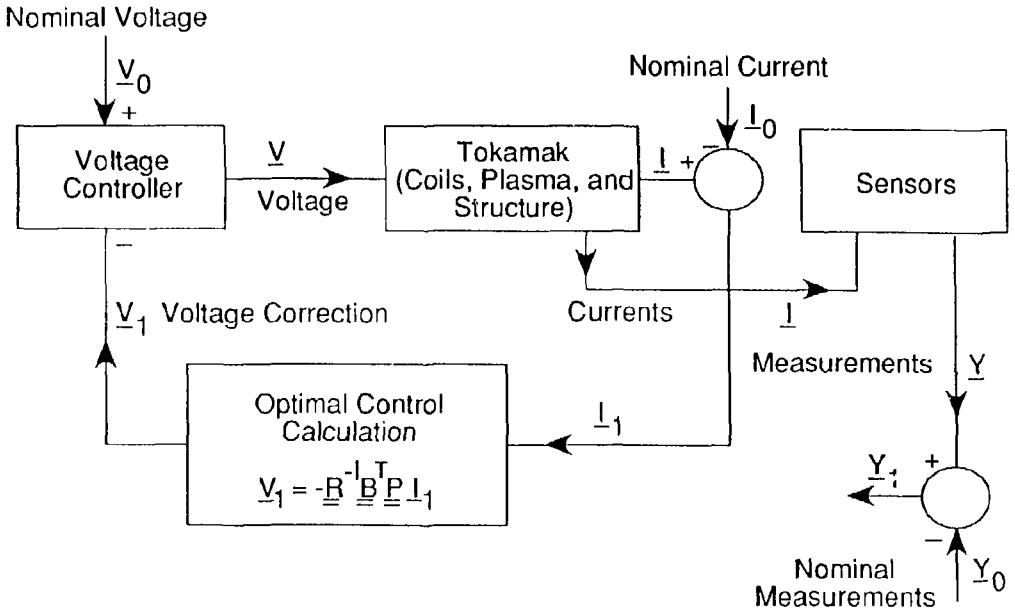
Nominal Voltage
$\underline{V}_0$
+
Voltage Controller
$\underline{V}$
Voltage
Tokamak (Coils, Plasma, and Structure)
Nominal Current
$\underline{I}_0$
$\underline{I}$ +
−
Sensors
−
$\underline{V}_1$ Voltage Correction
Currents
$\underline{I}$
Measurements
$\underline{Y}$
Optimal Control Calculation
$\underline{V}_1 = -\underline{\underline{R}}^{-1}\underline{\underline{B}}^T\underline{\underline{P}}\,\underline{I}_1$
$\underline{I}_1$
$\underline{Y}_1$
+
−
Nominal Measurements
$\underline{Y}_0$

Fig. 3

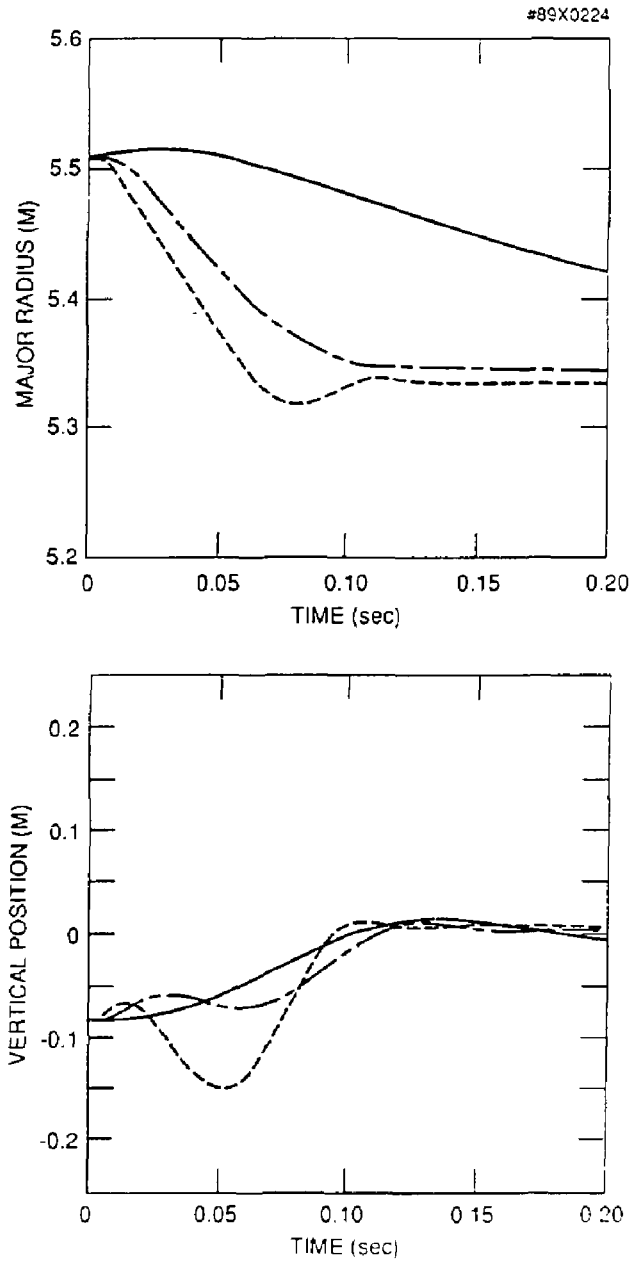
#89X0224
5.6
5.5
5.4
5.3
5.2
MAJOR RADIUS (M)
0
0.05
0.10
0.15
0.20
TIME (sec)
0.2
0.1
0
-0.1
-0.2
VERTICAL POSITION (M)
0
0.05
0.10
0.15
0.20
TIME (sec)

Fig. 4

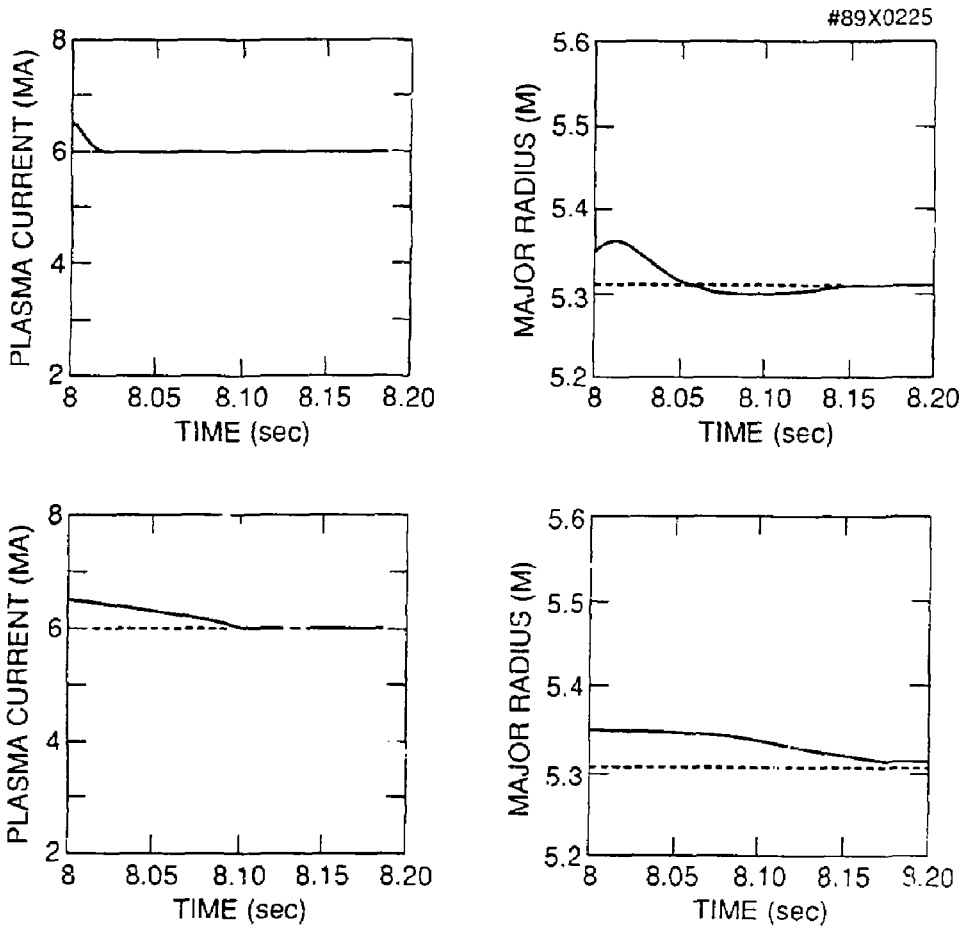
#89X0225
PLASMA CURRENT (MA)
8
6
4
2
8
8.05
8.10
8.15
8.20
TIME (sec)
MAJOR RADIUS (M)
5.6
5.5
5.4
5.3
5.2
8
8.05
8.10
8.15
8.20
TIME (sec)
PLASMA CURRENT (MA)
8
6
4
2
8
8.05
8.10
8.15
8.20
TIME (sec)
MAJOR RADIUS (M)
5.6
5.5
5.4
5.3
5.2
8
8.05
8.10
8.15
8.20
TIME (sec)

Fig. 5

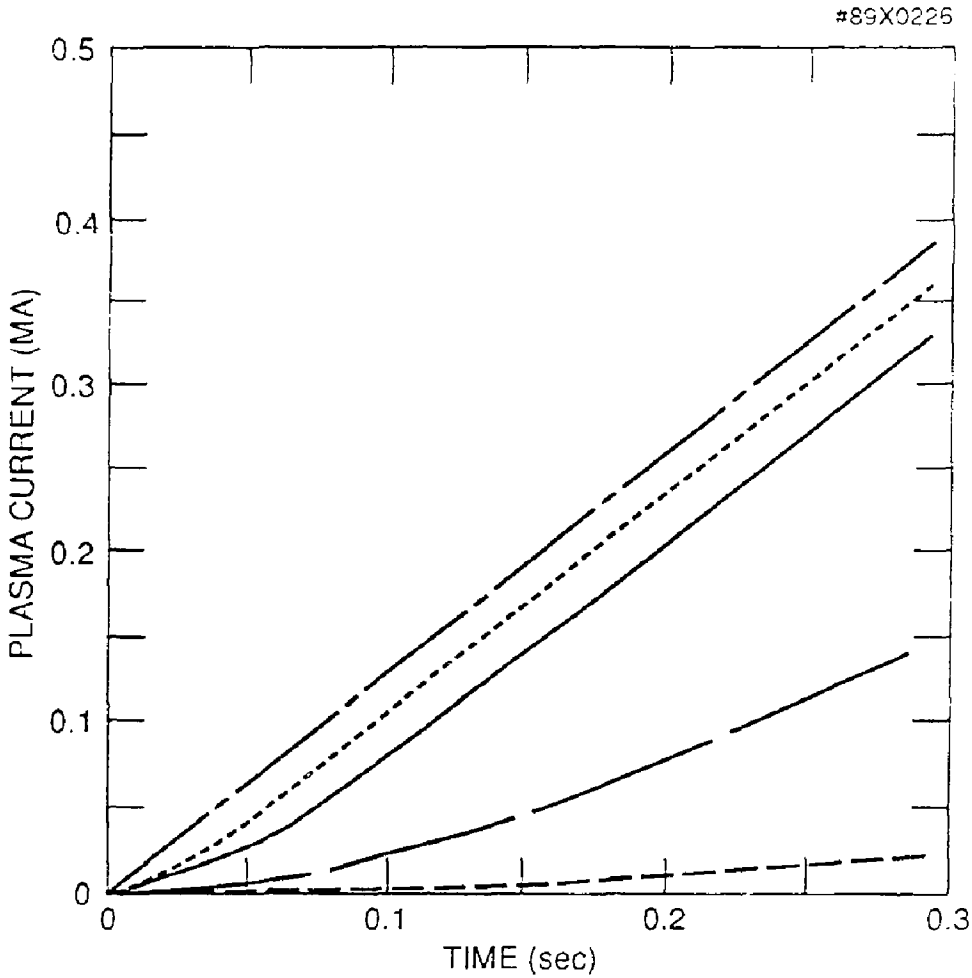

Fig. 6

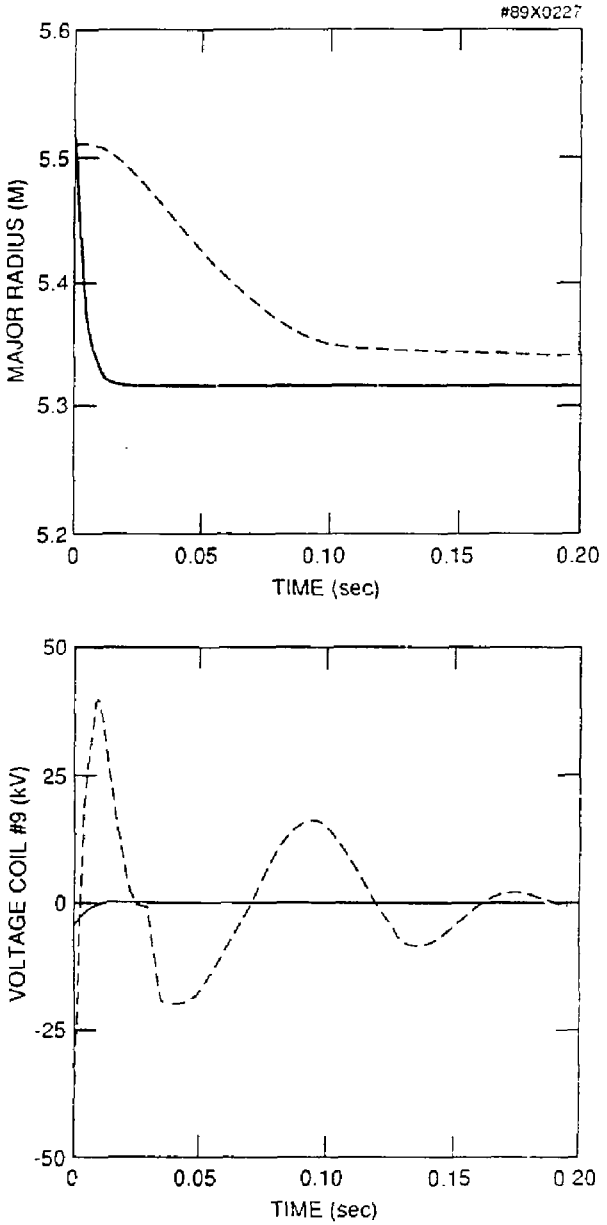
#89X0227
5.6
5.5
5.4
5.3
5.2
MAJOR RADIUS (M)
0
0.05
0.10
0.15
0.20
TIME (sec)
50
25
0
-25
-50
VOLTAGE COIL #9 (kV)
0
0.05
0.10
0.15
0.20
TIME (sec)

Fig. 7

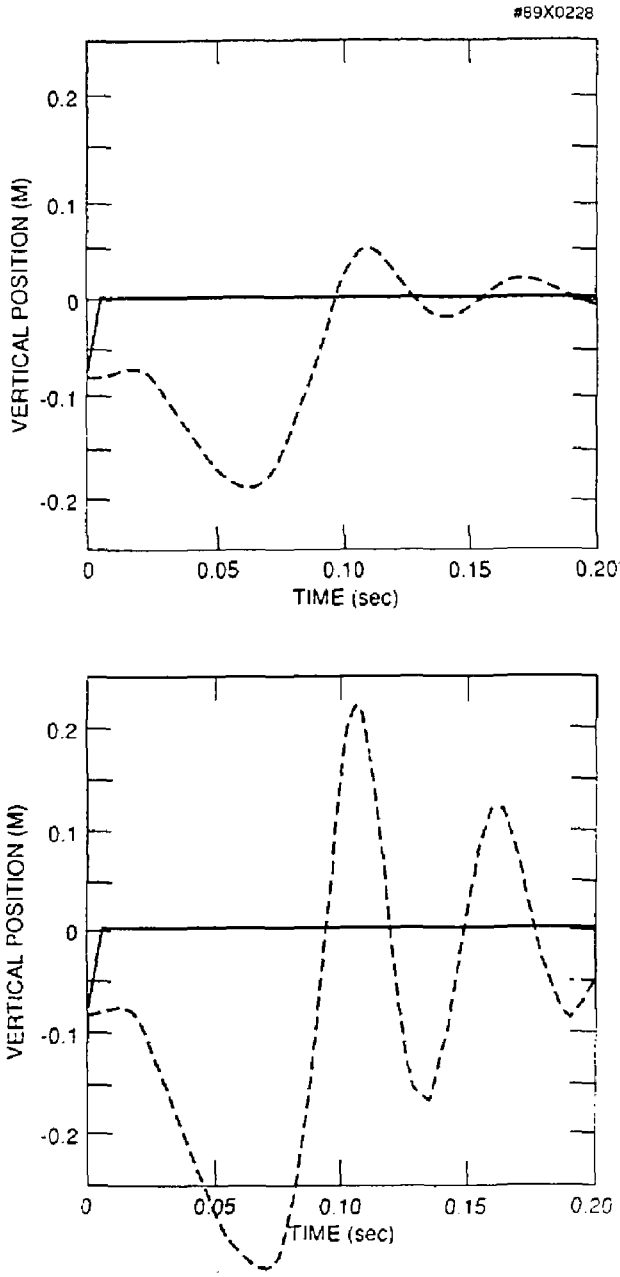
#89X0228
VERTICAL POSITION (M)
0.2
0.1
0
-0.1
-0.2
0
0.05
0.10
0.15
0.20
TIME (sec)
VERTICAL POSITION (M)
0.2
0.1
0
-0.1
-0.2
0
0.05
0.10
0.15
0.20
TIME (sec)

Fig. 8

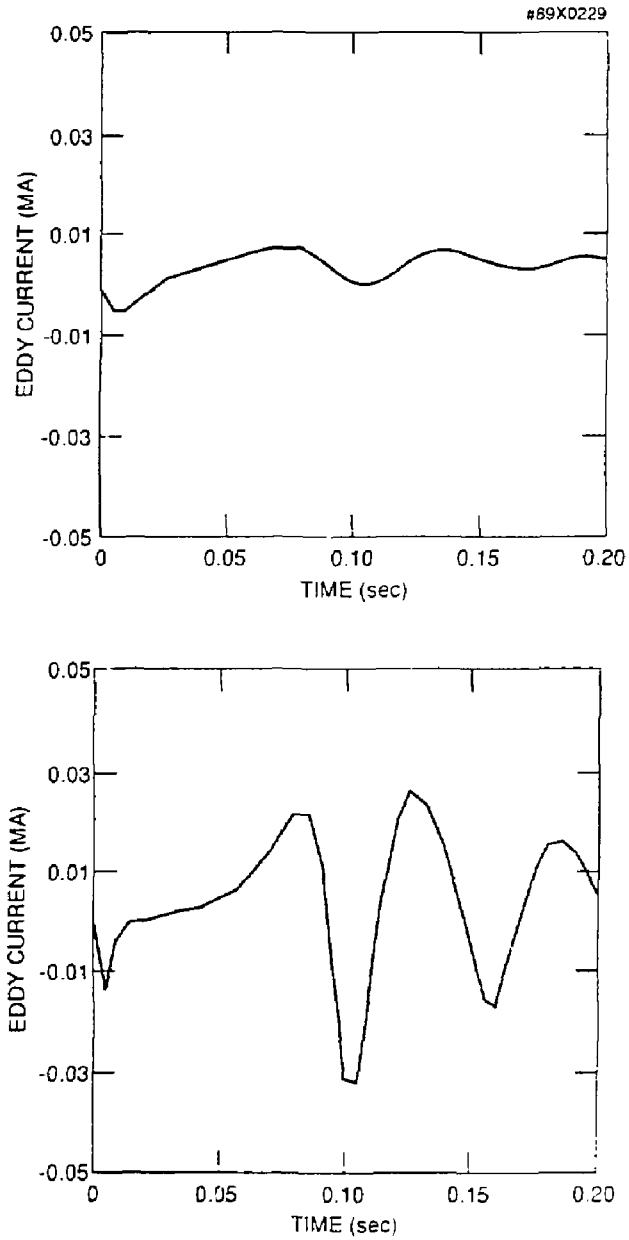
#89X0229
0.05
0.03
0.01
-0.01
-0.03
-0.05
EDDY CURRENT (MA)
0
0.05
0.10
0.15
0.20
TIME (sec)
0.05
0.03
0.01
-0.01
-0.03
-0.05
EDDY CURRENT (MA)
0
0.05
0.10
0.15
0.20
TIME (sec)

Fig. 9

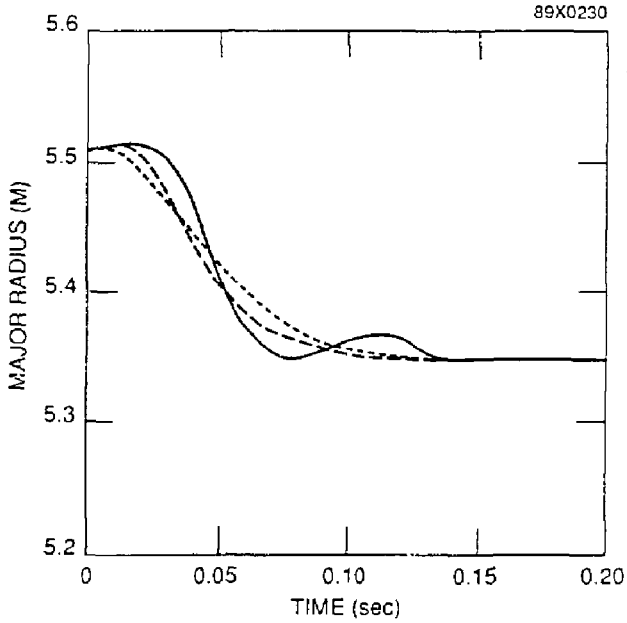
89X0230
5.6
5.5
5.4
5.3
5.2
MAJOR RADIUS (M)
0
0.05
0.10
0.15
0.20
TIME (sec)

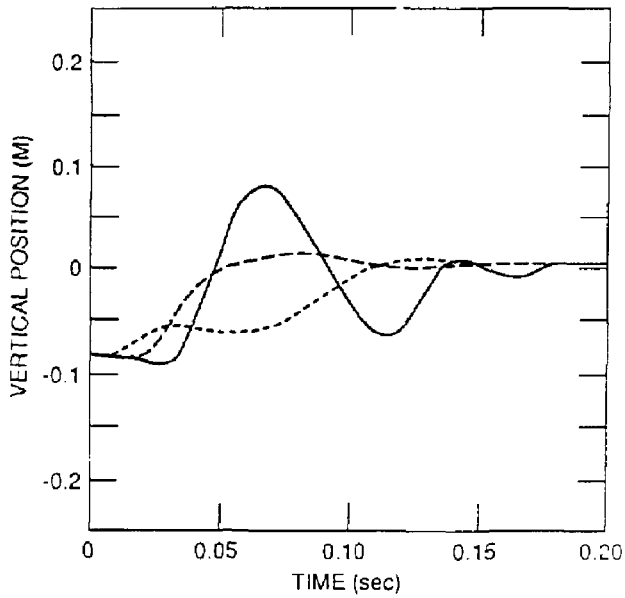
0.2
0.1
0
-0.1
-0.2
VERTICAL POSITION (M)
0
0.05
0.10
0.15
0.20
TIME (sec)

Fig. 10

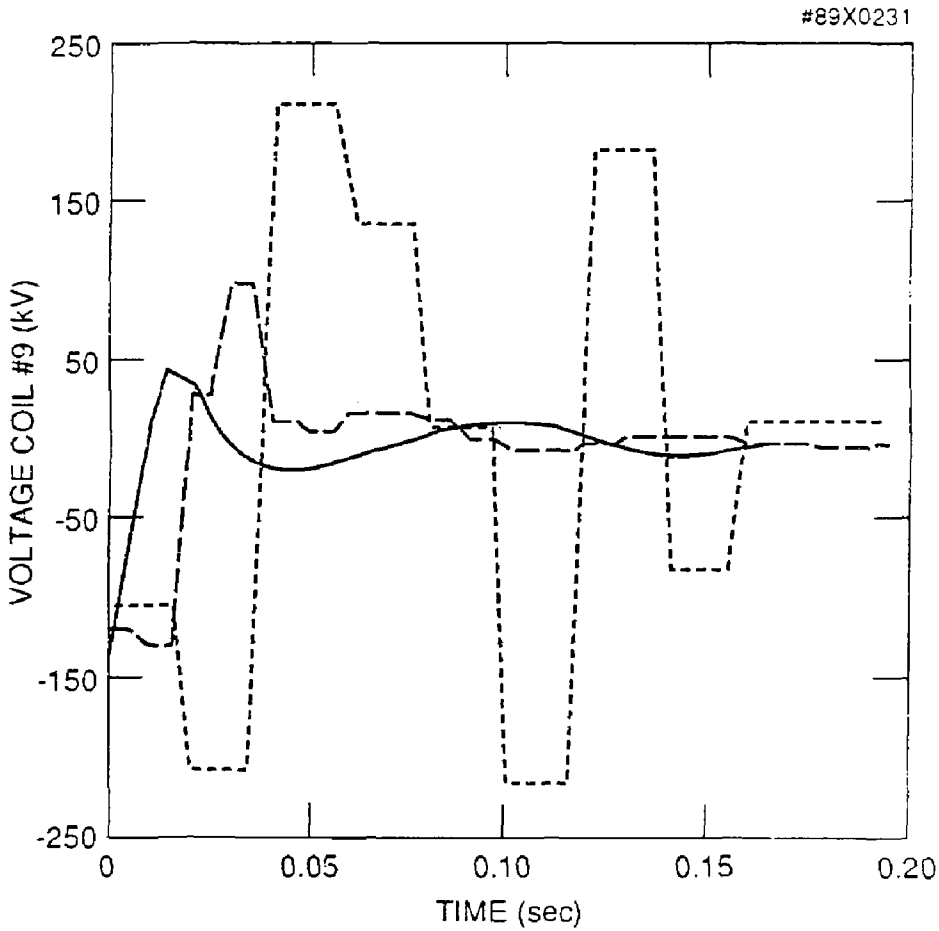
#89X0231
250
150
50
-50
-150
-250
VOLTAGE COIL #9 (kV)
0
0.05
0.10
0.15
0.20
TIME (sec)

Fig. 11

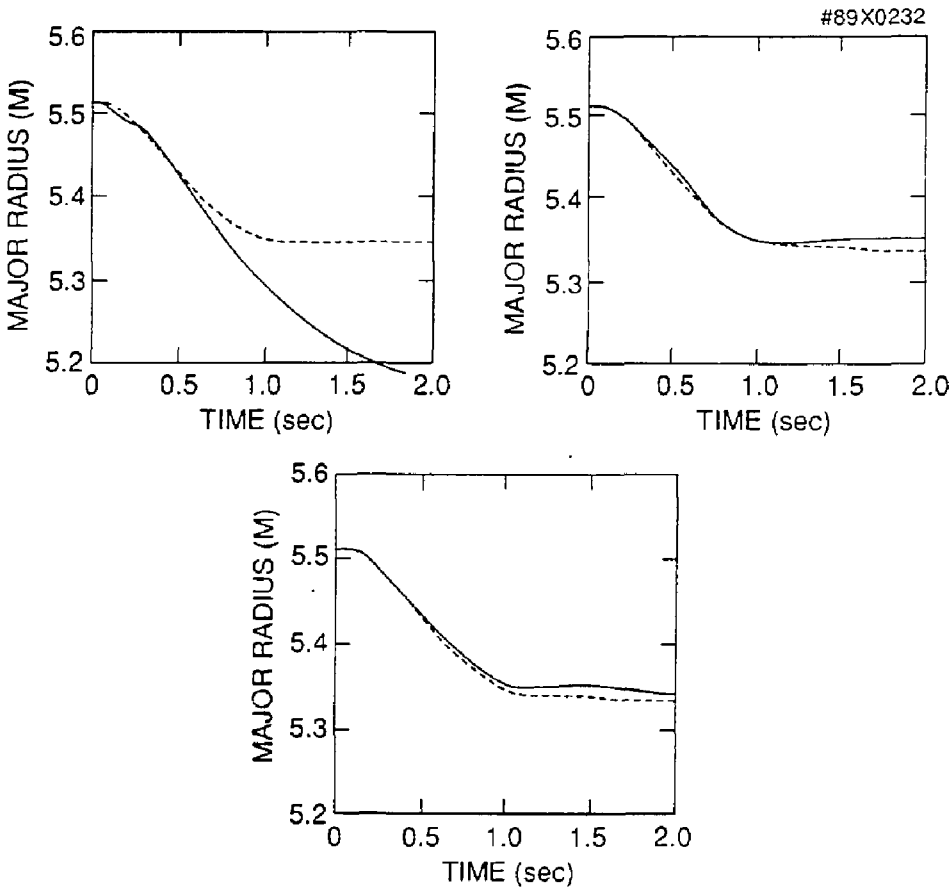

Fig. 12

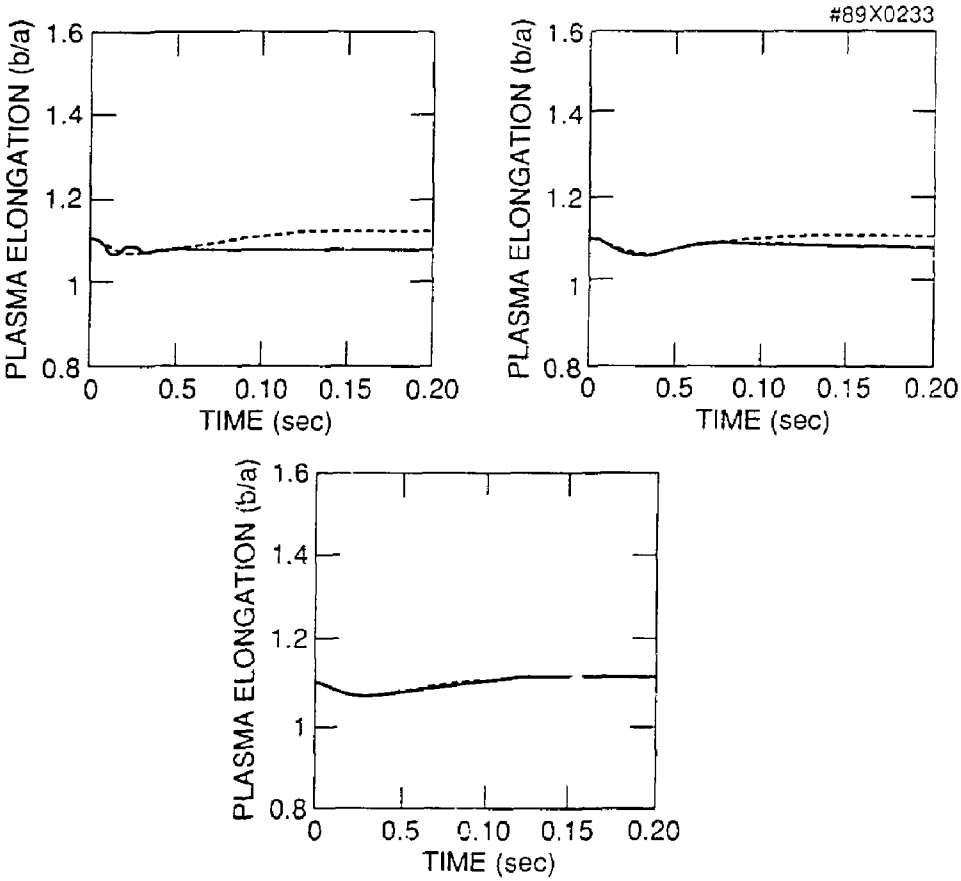
#89X0233
PLASMA ELONGATION (b/a)
1.6
1.4
1.2
1
0.8
0
0.5
0.10
0.15
0.20
TIME (sec)

Fig. 13

EXTERNAL DISTRIBUTION IN ADDITION TO UC-420

Dr. Frank J. Paoloni, Univ of Wollongong, AUSTRALIA
Prof. M.H. Brennan, Univ Sydney, AUSTRALIA
Plasma Research Lab., Australian Nat. Univ., AUSTRALIA
Prof. I.R. Jones, Flinders Univ., AUSTRALIA
Prof. F. Cap, Inst Theo Phys, AUSTRIA
Prof. M. Heindler, Instut fur Theoretische Physik, AUSTRIA
M. Goossens, Astronomisch Instituut, BELGIUM
Ecole Royale Militaire, Lab de Phys Plasmas, BELGIUM
Commission-European, Dg-XII Fusion Prog, BELGIUM
Prof. R. Boucique, Rijksuniversiteit Gent, BELGIUM
Dr. P.H. Sakanaka, Instituto Fisica, BRAZIL
Instituto De Pesquisas Espaciais-INPE, BRAZIL
Documents Office, Atomic Energy of Canada Limited, CANADA
Dr. M.P. Bachynski, MPB Technologies, Inc., CANADA
Dr. H.M. Skarsgard, University of Saskatchewan, CANADA
Dr. H. Barnard, University of British Columbia, CANADA
Prof. J. Teichmann, Univ. of Montreal, CANADA
Prof. S.R. Sreenivasan, University of Calgary, CANADA
Prof. Tudor W. Johnston, INRS-Energie, CANADA
Dr. Bolton, Centre canadien de fusion magnetique, CANADA
Dr. C.R. James, Univ. of Alberta, CANADA
Dr. Peter Lukac, Komenskeho Univ, CZECHOSLOVAKIA
The Librarian, Culham Laboratory, ENGLAND
The Librarian, Rutherford Appleton Laboratory, ENGLAND
Mrs. S.A. Hutchinson, JET Library, ENGLAND
C. Mouttet, Lab. de Physique des Milieux Ionises, FRANCE
J. Radet, CEN/CADARACHE - Bat 506, FRANCE
Ms. C. Rinni, Librarian, Univ. of Ioannina, GREECE
Dr. Tom Mual, Academy Bibliographic Ser., HONG KONG
Preprint Library, Hungarian Academy of Sciences, HUNGARY
Dr. B. Das Gupta, Saha Inst of Nucl. Phys., INDIA
Dr. P. Kaw, Institute for Plasma Research, INDIA
Dr. Philip Rosenau, Israel Inst. of Tech, ISRAEL
Librarian, Int'l Ctr Theo Phys, ITALY
Prof. G. Rostagni, Istituto Gas Ionizzati Del CNR, ITALY
Miss Clelia De Palo, Assoc EURATOM-ENEA, ITALY
Dr. G. Grosso, Istituto di Fisica del Plasma, ITALY
Dr. H. Yamato, Toshiba Res & Dev, JAPAN
Prof. T. Kawakami, Atomic Energy Res. Institute, JAPAN
Prof. Kyoji Nishikawa, Univ of Hiroshima, JAPAN
Director, Dept. Large Tokamak Res. JAERI, JAPAN
Prof. Satoshi Itoh, Kyushu University, JAPAN
Research Info Center, Nagoya University, JAPAN
Prof. S. Tanaka, Kyoto University, JAPAN
Library, Kyoto University, JAPAN
Prof. Nobuyuki Inoue, University of Tokyo, JAPAN
S. Mori, JAERI, JAPAN
H. Jeong, Librarian, Korea Advanced Energy Res Inst, KOREA
Prof. D.I. Choi, The Korea Adv. Inst of Sci & Tech, KOREA
Prof. B.S. Liley, University of Waikato, NEW ZEALAND
Institute of Plasma Physics, PEOPLE'S REPUBLIC OF CHINA
Librarian, Institute of Phys., PEOPLE'S REPUBLIC OF CHINA
Library, Tsing Hua University, PEOPLE'S REPUBLIC OF CHINA
Z. Li, Southwest Inst. Physics, PEOPLE'S REPUBLIC OF CHINA
Prof. J.A.C. Cabral, Inst Superior Tecnico, PORTUGAL
Dr. Octavian Petrus, AL I CUZA University, ROMANIA
Dr. Jan de Villiers, Fusion Studies, AEC, SO AFRICA
Prof. M.A. Hellberg, University of Natal, SO AFRICA
C.I.E.M.A.T., Fusion Div. Library, SPAIN
Dr. Lennart Stenflo, University of UMEA, SWEDEN
Library, Royal Institute of Tech, SWEDEN
Prof. Hans Wilhelmson, Chalmers Univ of Tech, SWEDEN
Centre Phys des Plasmas, Ecole Polytech Fed, SWITZERLAND
Bibliotheek, Fom-Inst Voor Plasma-Fysica, THE NETHERLANDS
Metin Durgut, Middle East Technical University, TURKEY
Dr. O.D. Ryutov, Siberian Acad Sci, USSR
Dr. G.A. Eliseav, Kurchatov Institute, USSR
Dr. V.A. Glukhikh, Inst Electrophysical Apparatus, USSR
Prof. O.S. Padichenko, Inst. of Phys. & Tech. USSR
Dr. L.M. Kovrizhnykh, Institute of Gen. Physics, USSR
Nuclear Res. Establishment, Julich Ltd., W. GERMANY
Bibliothek, Inst. Fur Plasmaforschung, W. GERMANY
Dr. K. Schindler, Ruhr-Universitat Bochum, W. GERMANY
ASDEX Reading Rm, c/o Wagner, IPP/Max-Planck, W. GERMANY
Librarian, Max-Planck Institut, W. GERMANY
Prof. R.K. Janev, Inst of Phys, YUGOSLAVIA